

The AstraLux Multiplicity Survey: Extension to Late M-dwarfs*

Markus Janson^{1,2}, Carolina Bergfors^{2,3}, Wolfgang Brandner², Natalia Kudryavtseva^{2,4}, Felix Hormuth², Stefan Hippler², Thomas Henning²

ABSTRACT

The distribution of multiplicity among low-mass stars is a key issue to understanding the formation of stars and brown dwarfs, and recent surveys have yielded large enough samples of nearby low-mass stars to study this issue statistically to good accuracy. Previously, we have presented a multiplicity study of ~ 700 early/mid M-type stars observed with the AstraLux high-resolution Lucky Imaging cameras. Here, we extend the study of multiplicity in M-type stars through studying 286 nearby mid/late M-type stars, bridging the gap between our previous study and multiplicity studies of brown dwarfs. Most of the targets have been observed more than once, allowing us to assess common proper motion to confirm companionship. We detect 68 confirmed or probable companions in 66 systems, of which 41 were previously undiscovered. Detections are made down to the resolution limit of ~ 100 mas of the instrument. The raw multiplicity in the AstraLux sensitivity range is 17.9%, leading to a total multiplicity fraction of 21–27% depending on the mass ratio distribution, which is consistent with being flat down to mass ratios of ~ 0.4 , but cannot be stringently constrained below this value. The semi-major axis distribution is well represented by a log-normal function with $\mu_a = 0.78$ and $\sigma_a = 0.47$, which is narrower and peaked at smaller separations than for a Sun-like sample. This is consistent with a steady decrease in average semi-major axis from the highest-mass binary stars to the brown dwarf binaries.

Subject headings: binaries: general — techniques: high angular resolution — stars: late-type

1. Introduction

The multiplicity properties of stars hold clues to their formation and early evolution (e.g. Goodwin & Kroupa 2005; Marks & Kroupa 2011; Bate 2012), and binarity is of fundamental importance for a range of astrophysical applications, such as determination of physical properties and target selection for exoplanet studies. Consequently, detailed multiplicity studies have been performed over a wide range of stellar masses and ages (see e.g. Duchêne & Kraus 2013; Reipurth et al. 2014, for recent summaries). While multiplicity at the low-mass end – in the M-dwarf regime – has been a

subject of study for a long time (e.g. Fischer & Marcy 1992; Delfosse et al. 2004; Law et al. 2008), there have recently emerged reasons to revisit this subject. The main reason for this is that the nearby M-dwarf population is becoming increasingly well characterized. Recent studies have greatly increased our sample of securely identified M-dwarf stars in the Solar neighborhood (e.g. Riaz et al. 2006; Reid et al. 2007; Lépine & Gaidos 2011). Furthermore, while distances for this class of objects have previously been scarce due to the fact that they are generally too faint to have been observed by Hipparcos (Perryman et al. 1997), recent parallax studies have started to become increasingly complete to the lowest-mass stars (e.g. Henry et al. 2006; Dittmann et al. 2014; Reidel et al. 2014). Hence, larger well-defined statistical samples can be studied than has been possible before, and a greater accuracy is achievable in the characterization of their properties.

The AstraLux Norte (Hormuth 2007; Hormuth et al. 2008) and Sur (Hippler et al. 2009) cameras are well

*Based on observations collected at the Centro Astronómico Hispano Alemán (CAHA) at Calar Alto, operated jointly by the Max-Planck Institute for Astronomy and the Instituto de Astrofísica de Andalucía (CSIC).

¹Queen's University Belfast, Belfast, Northern Ireland, UK; m.janson@qub.ac.uk

²Max Planck Institute for Astronomy, Heidelberg, Germany

³University College London, London, UK

⁴Astronomisches Rechnen-Institut, Heidelberg, Germany

suited for multiplicity studies by use of high-resolution imaging (e.g. Hormuth et al. 2007; Daemgen et al. 2009; Peter et al. 2012; Bergfors et al. 2013), with a resolving power of approximately 100 mas. AstraLux is a high speed and low read noise camera used for the purpose of so-called Lucky Imaging (e.g. Tubbs et al. 2002; Law et al. 2006). Previously, we have used this instrument for the study of multiplicity in primarily early-type M-dwarfs (Bergfors et al. 2010; Janson et al. 2012). In the summary study of 2012 (Janson et al. 2012), we found that the multiplicity properties of these stars were largely consistent with being continuously intermediate between the Sun-like (Raghavan et al. 2010) and brown dwarf (Burgasser et al. 2007) populations, though possibly with the exception of the mass ratio distribution (see also Reggiani & Meyer 2013; Goodwin 2013). The apparent continuities and discontinuities motivate further study of a later-type sample, bridging the gap between early/mid M-dwarfs in Janson et al. (2012) and very low-mass (VLM) stars and brown dwarfs in Burgasser et al. (2007). The sample presented in Lépine & Gaidos (2011) provides an excellent basis for this purpose. Here we will present a study of multiplicity in mid/late M-type stars (primarily M3 and later, down to M8), which overlaps with both the previous M-dwarf and VLM studies.

In the following, we will first discuss the sample properties in Sect. 2, and then the observations and data reductions in Sect. 3. This will be followed by a summary of the results in Sect. 5 and a description of the statistical properties of the sample in Sect. 6. Finally, we will discuss the implications of this study in the context of multiplicity across all stellar masses in Sect. 8 and summarize the conclusions in Sect. 9.

2. Target sample

2.1. Observational properties

The targets in this study were selected from the (Lépine & Gaidos 2011) sample, where stars with a spectral type (SpT) estimate of M5 or later were selected if they were sufficiently bright ($J \leq 10.0$ mag) and sufficiently far North ($>-15^\circ$) to be meaningfully observed with AstraLux Norte. In total, this gave an input sample of 408 potential targets, of which 286 were actually observed. Targets from the ‘master list’ of 408 stars were chosen entirely on the basis of observability during a given run and limited by the total amount of telescope time available for the program,

hence the sub-selection of 286 actual targets can be seen as random, and should not introduce any selection effects in the analysis. The full set of observed targets is summarized in Table 1, where the basic observable quantities are from Lépine & Gaidos (2011) unless otherwise stated. In Lépine & Gaidos (2011), the SpT estimates were not spectroscopically determined, but merely inferred from the $V - J$ colors of the stars. For our study, we have cross-matched these SpT estimates with actual SpTs in the literature for all cases where such measurements exist, and found that the former estimates exhibit a systematic offset toward later spectral types. For 198 out of the 286 observed stars, literature SpT determinations exist. Among these 198 cases, the median difference between the two estimates is 1 spectral sub-type. While a few extreme cases exist, such as I04122+6443 which is classified as M5 in Lépine & Gaidos (2011) but M1 in Bender & Simon (2008), most stars are close to this 1 spectral sub-type offset. In Table 1, we adopt the literature SpT measurement for the 198 cases for which this is available, and denote the SpT with an upper case letter (e.g. ‘M5’). For the remaining 88 cases, we use the photometric estimations but label them with a lower case letter (e.g. ‘m5’), following the source notation. By analogy with the 198 overlapping cases, it is likely that the actual spectral type is approximately 1 spectral sub-type earlier than what the lower case notation implies for these 88 targets.

In 198 cases, we have been able to acquire trigonometric parallaxes. These have been provided from a range of studies, the references for which are summarized in Table 1. Photometric parallaxes were used in the remaining cases, as provided in Lépine & Gaidos (2011). Distances for the bulk of the sample range from 3 to 36 pc, with three targets at larger distances (40–70 pc). The median distance for the full sample is 15 pc. The 69% coverage (198 out of 286) of trigonometric parallaxes is a substantial improvement on previous M-star studies such as Janson et al. (2012), in which the vast majority of distances had to be estimated photometrically.

2.2. Physical properties

The fact that such a large fraction of the sample has trigonometric parallaxes is greatly beneficial for the estimation of semi-major axis distributions, as will be seen in Sect. 6.2. On the other hand, the estimation of mass ratio distributions is very challenging for this class of objects. For late M-type stars, a mass can-

not be reliably derived from spectral type alone, since the temperature of the object varies significantly during its long-lasting pre-main sequence phase¹. Instead, masses have to be inferred based on models with significant uncertainties. These models also require the age of the system as an additional parameter, which is itself also highly uncertain in most cases. A combination of evolutionary and atmospheric models are required to make predictions for photometric values in a given band for a given stellar mass at a given age. Here we use both the NextGen (Hauschildt et al. 1999) and the more recent BT-Settl (Allard 2014) atmospheric models, and the evolutionary models of Baraffe et al. (1998, 2003). The COND (Allard et al. 2001) models are used to fill in some extreme ranges of the parameter space not covered by the aforementioned models. Differences between different evolutionary models are small compared to the other uncertainties considered here (a few percent in luminosity for a given mass and age, see e.g. Burrows et al. 1997; Saumon & Marley 2008).

Upper and lower boundaries for the ages are estimated in the following way: If a certain target has been identified as a member of a young moving group in the literature, the age boundaries of the moving group are assigned to the target irrespective of any other characteristics. These are estimated as 10–20 Myr for the β Pic moving group (e.g. Zuckerman et al. 2001; Binks & Jenkins 2014) and 50–150 Myr for the AB Dor moving group (e.g. Luhman et al. 2005a; Janson et al. 2007). Likewise, if a target is not identified as a moving group member but it has been subjected to a detailed age analysis in the literature, the corresponding age boundaries are assigned. For all other targets, we apply a rough age estimate based solely on their X-ray luminosity (provided in Lépine & Gaidos 2011). If a target has a value of L_X/L_{bol} comparable to the values of the targets studies in Shkolnik et al. (2012), it is assumed to have an age in the same range, and thus assigned 30 Myr as a lower bound and 300 Myr as an upper bound. If the value is lower but there is still detectable X-ray emission, the target is assumed to be older but still part of a young population with a lower bound of 300 Myr and an upper bound of 1 Gyr. If no X-ray emission is detected, it is assumed to be a field star with an age between 1 Gyr and 10 Gyr. The broad

¹The pre-main sequence lasts about 180 Myr for a 0.2 M_{sun} star, 500 Myr for a 0.1 M_{sun} star, and 3 Gyr for a 0.075 M_{sun} star (e.g. Burrows et al. 1993, 1997; Baraffe et al. 1998).

ranges are meant to encompass the fact that the uncertainties in the age determination are inevitably very large. Nonetheless, we strongly caution against taking the quoted age range for any individual target at face value; they should only be considered as broad general age assignments to the population, in order to benefit the statistical analysis.

3. Observations and Data Reduction

All observations in this program were acquired with the AstraLux Norte camera on the 2.2m telescope at Calar Alto in Spain. The 2.2m telescope is on an equatorial mount. AstraLux uses an Andor DV887-UVB camera head equipped with a thinned, back-illuminated, electron-multiplying 512x512 pixel monolithic CCD. The CCD is equipped with two readout registers, one for conventional readout, and one 536 stage electron multiplication register. Each of the two registers comes with its own output amplifier. All Lucky Imaging data were obtained using the electron multiplication mode, and the associated output amplifier. The camera allows to select electron multiplication gains of up to 2500. For astronomical observations, the gain values are typically selected such that the ADU counts in the brightest pixel do not exceed 50% of the linearity limit of the camera. It has been verified in lab experiments that charge transfer efficiency does not have any impact on the astrometric accuracy. Typical observations are made using a 256 by 256 pixel window readout, which facilitates shorter single frame integration times. The window also allows to avoid column 244 of the detector, which is subject to a charge trap that traps a few electron per clock cycle. Apart from column 244, the CCD has very good cosmetics without any clusters of bad pixels. The raw pixel scale (before oversampling; see below) is approximately 46 mas/pixel on average.

The observations were carried out in six separate runs: On 8–9 Nov 2011, on 5–8 Jan 2012, on 6–7 Jun 2012, on 27–29 Aug 2012, on 3 Sept 2012, and on 22–24 Nov 2012. Each target was observed in both the i' -band and the z' -band, and a large fraction of the targets, including the singles, were observed in two or more separate epochs. In total, excluding calibration observations, approximately 940 observations were acquired for the purpose of this survey, covering the 286 individual targets. As per usual, observing conditions varied during the runs, but since so many targets were observed several times, there is in general

at least one frame of acceptable quality per star. The typical full width at half maximum (FWHM) is close to 100 mas, which is an appropriate measure for the resolving power of this instrument. For the purpose of astrometric calibration, we observed either the Trapezium or M15, depending on the season during which the observations were performed. The astrometric calibration is described in more detail in Sect. 4.

Although the field of view of AstraLux Norte can be as large as $23''$ across with the full frame in use, many of the images were taken with a subarray readout and the target was not always centered perfectly in the frame, so the fully complete region has a radius of $5''$ around each star. We will thus only consider companions inside of $5''$ for statistical purposes in this study.

The basic data reduction makes use of the pipeline developed specifically for the purpose, described in Hormuth et al. (2008). The pipeline performs flat fielding and bias correction of the data, followed by a drizzle algorithm to oversample the image by a factor of two, for a final pixel scale of approximately 23 mas/pixel. Individual frames are then aligned based on the brightest pixel in the oversampled image, and the re-aligned images are subsequently recombined into collapsed images. By default, the pipeline produces four different reduced frames per full observation, corresponding to different cut-offs for the selection of frames used. In this study, we consistently used the selection in which the 10% best frames were included in the collapsed frame. Individual frame exposure times were typically 30 ms, with minor variations depending on observing conditions and target brightness. The total number of frames was always selected so that the total integration time would add up to 300 s. Hence, the typical number of frames acquired was 10000, leading to a 10% selection of 1000 frames, adding up to 30 s of ‘useful’ integration time.

4. Astrometry and photometry

Astrometry was first calculated in detector coordinates, and subsequently translated into sky coordinates using the calibration observations of the Trapezium or M15. For the calibration data, we chose five of the brightest stars in the field, determined their relative positions using Gaussian centroiding, and compared to the relative locations of these stars in van der Marel et al. (2002) for M15 and McCaughrean et al. (1994) for Trapezium. We

also compared the results with a calibration based on the IRAF *geomap* procedure (see e.g. Köhler et al. 2008), and found that calibration within a given observing run was consistent to within 1% in pixel scale and 0.3° in position angle, regardless of choice of calibration method and selection of stars within the method. In this way, it was found that the pixel scale and orientation of true North in the respective runs were: 23.57 mas/pixel and 1.66° in Nov 2011, 23.58 mas/pixel and 1.72° in Jan 2012, 23.67 mas/pixel and 1.90° in Jun 2012, 22.59 mas/pixel and 1.83° in Aug 2012, 22.69 mas/pixel and 1.96° in Sept 2012, and 22.67 mas/pixel and 1.85° in Nov 2012. The calibration errors are dominated by the 1% uncertainty in pixel scale and the 0.3° uncertainty in position angle mentioned above, which we adopt as the formal error bars in each case.

As in previous runs, astrometry for wide binaries in the sample was determined using Gaussian centroiding, and astrometry for close binaries was determined using PSF fitting (Bergfors et al. 2010). Three PSFs were used in each case, to provide a well-defined mean and scatter in the PSF fitting. The PSFs were chosen among single stars in the survey to represent a broad range in observing conditions. In principle, one might tailor the PSF templates to each given target, such that only PSFs acquired under similar conditions are used in the fitting scheme. However, given the complex multi-modal variations of the PSF and the rapidly varying conditions during the observing nights, this is impractical, and our experience implies that no significant gain is achieved through such a procedure. Even if an apparent improvement were achieved, it would also be dubious whether the resulting implied precision could be trusted, given the aforementioned PSF complexity. We therefore consider it a better strategy to reflect a representative range of instrumental PSF realizations in the fitting, so that the derived error bars robustly encompass these variations. While the FWHM does not change much between different PSFs, since this measure is dominated by the diffraction-limited PSF core, beyond the core there can be quite a bit of variation in the PSF, sometimes showing diffraction rings and other times just a smooth halo. Astrometric values for the various systems are provided in Table 2. Relative photometry was determined simultaneously with the astrometry, by measuring aperture photometry in the case of wide binaries, and the relative brightness of the PSFs fit to each component for close binaries. In the case of the so-called ‘false triple’

effect, which often occurs in Lucky Imaging shift-and-add analysis when a binary with components of about equal brightness is observed and produces a tertiary ghost feature (at the same separation from the primary as the secondary but on the opposite side), we fit for all three components in the PSF fitting procedure. The photometry of the individual components was then calculated in the same way as in Janson et al. (2012), as first implemented by Law (2006).

With the age estimates from Sect. 2 in hand and the photometry derived here, upper and lower bounds for the individual component masses in each candidate multiple system are determined in the following way: Given a certain age estimate (an upper or lower bound for given target), a grid of model values for each of $\Delta i'$, $\Delta z'$, and total M_J are calculated for every combination of possible primary and secondary masses covered by the parameter space of the theoretical atmospheric and evolutionary models². These model values are then compared to the actual measured values (with their measured error bars) for every real binary pair. The matching that provides the minimum χ^2 then determines the masses that are assigned to the pair. For each star, we generate four different mass estimates, and for each binary pair we separately generate four different mass ratio estimates. The four estimates correspond to all possible combinations of the two age extremes and the two model sets (NextGen and BT-Settl with associated evolutionary models, see Hauschildt et al. 1999; Baraffe et al. 1998, 2003; Allard 2014). The final values and errors are then taken as the mean and the standard deviation of these four values for each star and each pair. In this way, both age and model uncertainties are considered in the estimations. The age uncertainty is the dominant one, due to the wide adopted ranges in this quantity. It is important to note that while the uncertainties in the individual stellar masses are large, the uncertainties in their mass ratios ($q = m_B/m_A$) are substantially smaller. This is due to the fact that any error in the age or model affects the estimated mass of the primary and secondary in a very similar way. As a result, while the median uncertainties in the primary and secondary masses are 23% and 22% respectively, the median error in the mass ratio is only 8%. Table 3 includes the masses and mass ratios that have been derived with this procedure.

²Photometric values in the relevant bands are provided directly by the models, such that no additional conversions are necessary.

5. Detections and confirmations

Several both new and previously known companion candidates were detected in this survey, and many of them could be confirmed to share a common proper motion with the primary, confirming physical companionship. In total, 66 of the 286 systems were found to be either probable or confirmed multiples within the complete range of 5'' separation, 41 of which were new discoveries. Of all systems, most were binaries and only two were triple systems, one of which was previously known. However, as noted in the individual notes, some of the systems are higher-order multiples when considering known companions outside of the AstraLux detectability range. Indeed, the system I08316+1932 is in reality a quintuple system, which is described in more detail in the individual notes. Several of the companions are probable brown dwarfs. A few examples of detected multiples are shown in Fig. 1.

For the candidates that were either observed twice with AstraLux or were already reported in previous imaging surveys, it was possible to test for common proper motion. Since these targets are very nearby and therefore have large proper motions in general, such a determination is possible even over rather short baselines. Our test followed the same structure as in Janson et al. (2012) – based on the location of a given candidate in one epoch relative to the primary star (in terms of separation and position angle), we made a prediction based on its proper motion and parallax of where it would occur in the second epoch if it were a static background object, and compared it to the actual measured position in the second epoch. If the locations were more than 3σ discrepant, common proper motion was considered as confirmed. For candidates that passed this test, we also made a test for measurable orbital motion by testing if the first and second epoch positions differed from each other by more than 3σ . If so, we considered orbital motion as confirmed as well. These evaluations were based on the motion between the first and last listed data points for each given target listed in Table 2, since this maximizes the observational baseline. After applying both tests, 37 candidates could be confirmed as bona fide companions, of which 33 also showed significant orbital motion. Three candidates could be discarded as background objects.

A color test was applied to all 37 single-epoch candidates, in which it was checked whether the $\Delta i'$ and

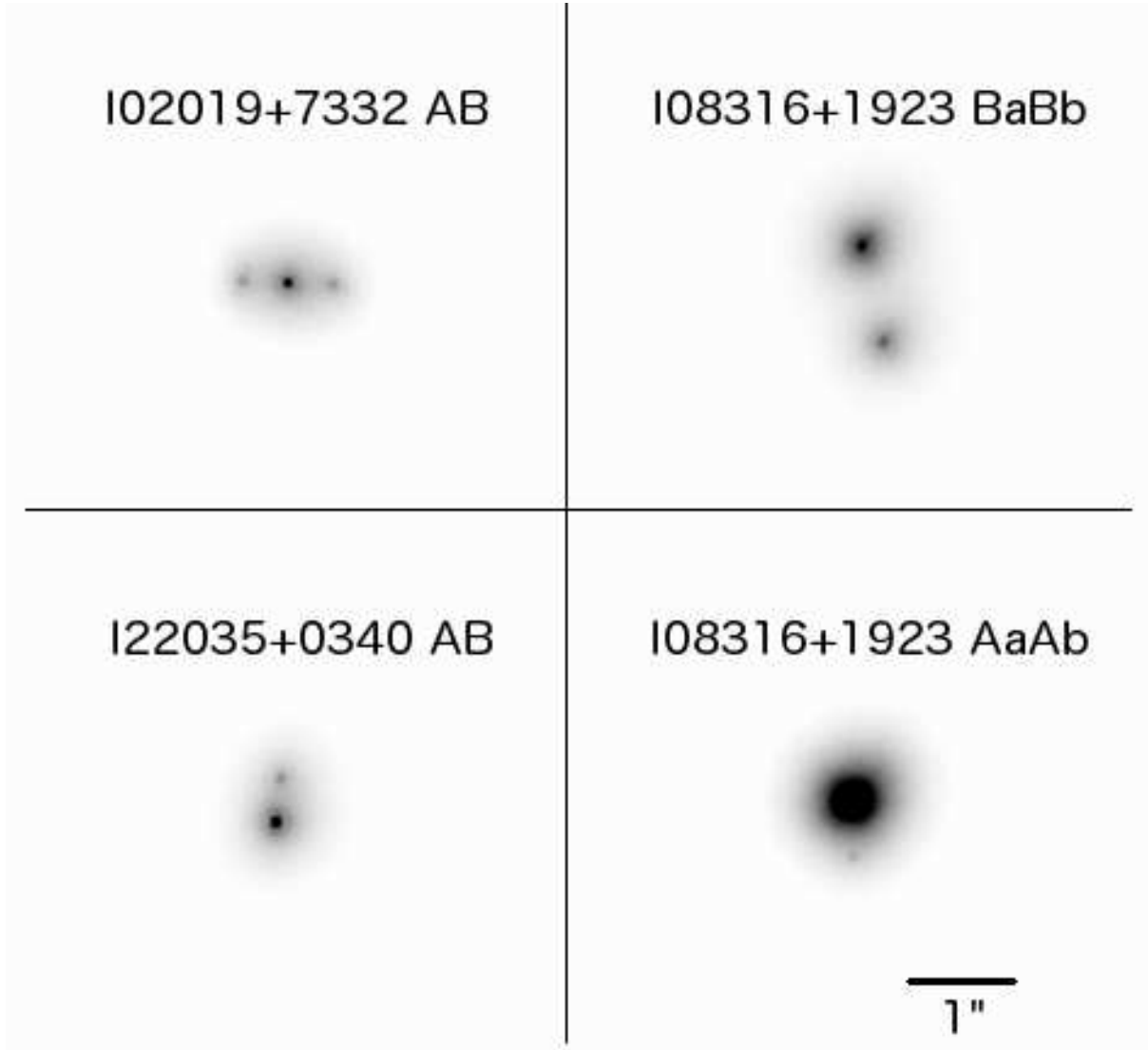


Fig. 1.— Examples of multiples discovered with AstraLux in this survey. Top left: A close binary displaying the false triple effect that is common in such systems. Bottom left: A close binary without false triple effects. Top right: The Northern pair of the quintuple system I08316+1923, also known as GJ 2069. Bottom right: The Southern pair (with an additional unresolved companion to the Aa component) of the same quintuple system. The component farthest to the South marks a limiting case for what can be achieved with AstraLux Norte at this small separation. North is up and East is to the left in all images.

$\Delta z'$ yielded consistent results for an expected secondary. The same test was applied to one candidate for which two epochs of data exist, but where the baseline is insufficient for a conclusive proper motion test to be made. In this way, 33 candidates were found to have colors consistent with real companions. Five candidates were too blue to be low-mass stellar companions ($\Delta z' - \Delta i' > 0$, which would imply that the secondary is bluer than the primary), and thus discarded as likely background contaminants, although astrometric follow-up in the future will still be valuable for such candidates, in order to test whether there could be white dwarf companions among them. Even for many of the candidates that have only been observed or detected in one epoch, it is possible to draw conclusions about common proper motion. The targets move rapidly across the sky (from ~ 100 mas/yr to several hundreds of mas/yr), and have been observed in previous all-sky surveys spanning decades backward in time. Hence, any background contaminant that happens to end up close to the primary star at the AstraLux epoch should be separated from it by up to several arcseconds in those previous epochs of data. Hence, they are often detectable there, despite the much worse spatial resolution of wide-field surveys, and so from their presence or absence in the archival data, it can be determined whether or not they share a common proper motion with the primary. We have used archival data from primarily two surveys for this purpose: The Two Micron All Sky Survey (2MASS, see Skrutskie et al. 2006) and the first Palomar Observatory Sky Survey (POSS). Since 2MASS was performed in the late nineties up across the millennial shift, it provides up to a 15 year baseline, and a quite reasonable spatial resolution for a wide-field survey. However, while POSS has a slightly worse spatial resolution, it is the most useful survey for this purpose. This is due to the fact that it was performed largely in the early 1950s, providing a 60 year baseline for the vast majority of the targets. Since the candidates are bright, sensitivity is not a limiting issue for these purposes, but the most important issue is how far a background contaminant would have traveled relative to the primary since the archival epoch, hence why a large baseline is preferred. By examining these archival data sets, we were able to conclude for 24 targets that if the candidate were a background contaminant, it would have been clearly visible in the images. Since they are not there, we can infer that the candidates are physical companions that share a common proper motion with

the primary. In most of the 9 remaining cases (which are generally the targets that have the slowest proper motions and/or the faintest companions), a background contaminant would have been marginally detectable, but for any such limit case, we count common proper motion as not having been proven yet.

The vast majority (and probably all) of these 9 remaining cases are expected to be real companions. Aside from the high confirmation rate in the candidates for which a proper motion test has been performed, this can also be deduced from the fact that the distribution of the candidates in projected separation is strongly slanted toward small separations, while the opposite would be true in a sample dominated by background contaminants. They also all pass the color test mentioned above, matching the expectation for physical companions, which would be rare for background contaminants, since the blackbody flux peak sweeps across the $i' - z'$ wavelength range in the M-dwarf regime. In total, we thus consider 68 candidates in 66 systems to be either probable or confirmed physical companions.

The detections are plotted in Fig. 2, and the binary properties are summarized in tables 2 and 3.

6. Statistical analysis

6.1. Multiplicity fraction

In order to translate the 66/286 multiple systems into an actual multiplicity fraction, we need to take a number of subtle bias and selection effects into account. One of the most important factors in this regard is the brightness-limited nature of the sample. We imposed a constraint of 10 mag in J -band when selecting the targets. This will cause an excess of binaries in the sample, because for some binaries, the primary will be fainter than 10 mag, but the sum of the primary plus secondary light will be brighter than this limit. Hence, these binaries will be selected into the sample only because they are binaries, and would not have been selected if they were single. We can account for this effect by identifying those binaries that have been positively selected for, and simply removing them from the sample for the purpose of calculating a multiplicity fraction³. This is done by calculating individual J -band magnitudes for each component of each multiple

³We also note that if this correction is not done, there will be an artificial strong peak toward near-equal masses in the mass ratio distribution, as we demonstrated in Janson et al. (2012)

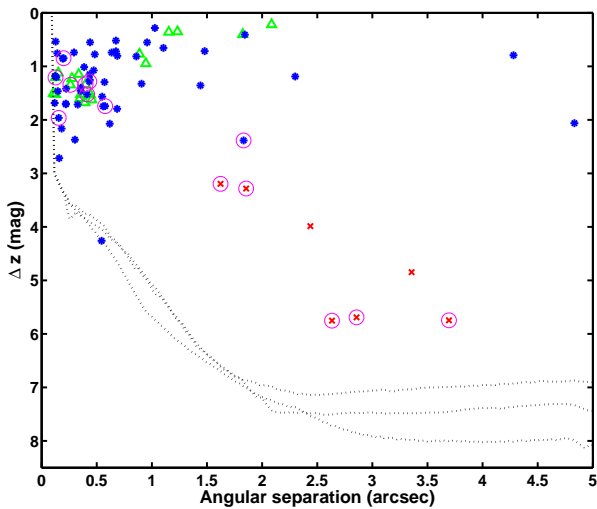


Fig. 2.— Plot of the AstraLux detections in angular separation versus $\Delta z'$. Red crosses are confirmed or suspected background stars. Green triangles are confirmed or probable binaries that are estimated as having been positively selected for (i.e., that would have been too faint to make the selection cut if the primary had been single). The blue asterisks are the ‘statistically clean’ (see Sect. 6.1) confirmed or probable binaries. Pairs for which either physical companionship or background contamination is probable but has not yet been demonstrated through common proper motion are encircled in magenta. Also plotted are the median contrast curves for the faint (top), intermediate (middle) and bright (bottom) targets (see text).

system, using the measured $\Delta z'$ as a proxy for the ΔJ value, and discarding those cases for which the primary J -band magnitude becomes fainter than 10 mag. A total of 18 systems are found to have been positively selected for, which leaves a sample in which 48 out of 268 systems are multiple (referred to henceforth as the ‘statistically cleaned’ sample). This results in a multiplicity fraction inside of the AstraLux sensitivity range of $48/268 = 17.9\%$.

In order to estimate a total multiplicity fraction that is independent of the AstraLux sensitivity, an assumption of the underlying distributions in mass ratio and semi-major axis needs to be made, and the corresponding population needs to be related to the AstraLux sensitivity space in order to evaluate what fraction of binaries fall into this space (the ‘detectable fraction’) and which fraction does not. As we will see, this is a complicated issue for this type of sample, where the mass ratio distribution is unconstrained for small mass ratios. Given the range of distributions that fit the data as discussed in Sect. 7, the detectable fraction probably lies between 66.6% and 85.4%. This gives a range of possible multiplicity fractions from $48/268/0.854 = 21.0\%$ to $48/268/0.666 = 26.9\%$. Hence, the uncertainty on the multiplicity fraction arising from the unknown mass ratio distribution is comparable to the random (Poisson distributed) error, which is approximately $\pm 3\%$.

6.2. Semi-major axis distribution

Given that a significant fraction of the stars in our sample have trigonometric parallaxes, we can establish good projected physical separations in general, which benefits the purpose of determining a well-constrained semi-major axis distribution. For translating between projected physical separation and semi-major axis, we use the same conversion factor of close to 1 as in Janson et al. (2013), based on the derivation of Brandeker et al. (2006) for a typical eccentricity distribution of $f(e) \sim 2e$. Our procedure for determining the semi-major axis distribution is based on generating a simulated population with a certain distribution, subjecting it to the sensitivity limits of AstraLux, and testing how well the resulting sample matches the actual body of detections, using a Kolmogorov-Smirnov test.

To begin with, we will assume that the sample has a uniform mass distribution, but later on we will discuss how changing the mass ratio distribution affects

these results. As input distributions for the semi-major axes (in units of AU here), we choose log-normal functions, both since this is the usual choice in this type of study (e.g. Duquennoy & Mayor 1991; Raghavan et al. 2010; Janson et al. 2012) and since it a priori appears to potentially provide a good fit to the observed distribution (see Fig. 3). We then vary the σ_a and μ_a parameters of the distribution in steps of 0.01 and see how the choices in these parameters affect the quality of the fit to the observed distribution. The steps are performed in a grid where both the σ_a and μ_a values are varied simultaneously, in order to find the global maximum in fit quality. This is important since there is some covariance in these parameters, where (e.g.) a smaller σ_a can potentially be partly compensated for through a larger μ_a , and vice versa.

The outer boundary of the AstraLux sensitivity range is set by the 5'' completeness radius. The inner boundary is set by the resolving power of approximately 100 mas. In between, the detectability of a candidate is set by the brightness contrast of the candidate relative to the contrast curve of the instrument. Contrast curves are calculated in the same way as is typically done in imaging surveys for faint companions (e.g. Lafrenière et al. 2007; Janson et al. 2011), by taking the standard deviation in a series of annuli centered on the star with different radii to represent the σ at various separations from the star, and relating them to the measured flux of the star for representing the limiting contrast of detectability. A 5σ criterion is chosen as the basis for the contrast curves. Since the resulting contrast curve varies a bit with the brightness of the primary, we have divided the target stars into faint (9–10 mag), intermediate (8–9 mag) and bright (<8 mag). Representative contrast curves are then derived by taking the median of the contrast curves for all single stars in the survey in each brightness category. The simulated populations are set to have the same brightness distribution as the full real sample, and so the detectability of companions around a given simulated star is evaluated based on the representative contrast curve for its particular brightness category. Any companion in the simulation that ends up inside of these completeness boundaries is counted as being detected, and any companion that does not is counted as a non-detection.

Finally, the separation distribution of ‘detected’ simulated companions is compared to the distribution of the actual detected sample. Every test is done 1000 times, and the median of the match probabil-

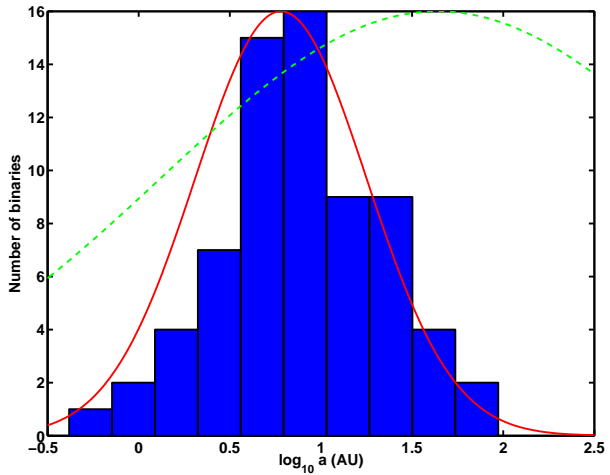


Fig. 3.— Distribution in semi-major axis of the sample. The histograms are the estimated semi-major axes of the observed sample. The red curve is the best-fit distribution in our simulations. Note that the simulations take into account the incompleteness effects at small separations, hence why the measured distribution sits lower than the model distribution at small separations. The green dashed curve is the corresponding distribution for Sun-like stars (Raghavan et al. 2010), which is clearly too broad and peaked at too large values to match this late M-dwarf sample.

ity of the 1000 tests is adopted (Babu & Feigelson 2006). For the log-normal distribution of the semi-major axis a in units of AU, we find that $\mu_a = 0.78$ and $\sigma_a = 0.47$ gives the best match to the observed distribution, with a match probability of 92.4%. As we mentioned previously, this is under the assumption of a uniform mass ratio distribution. If we instead choose a linearly increasing mass ratio distribution, the best-fit values become $\mu_a = 0.80$ and $\sigma_a = 0.48$ with a match probability of 92.5%. Hence, the result is not heavily dependent on the mass ratio distribution. The match probabilities as function of μ_a and σ_a for cross-sections in the parameter grid with values of ± 0.15 around the best-fit values are shown in Fig. 4, for both the cases of a uniform and a linearly increasing underlying mass ratio distribution.

7. Mass ratio distribution

As has been mentioned previously, the mass ratio distribution is very challenging to constrain. This is due to several reasons: 1) It is difficult to assign reliable masses to late M-type stars due to uncertainties in age and evolutionary models, although as we have seen in Sect. 2, this has a relatively small impact on the mass ratio. 2) The survey is incomplete for the smallest mass ratios, meaning that the distribution cannot be well constrained there. 3) There appears to be a bias avoiding near-equal brightnesses in close systems that are subject to the false triplet effect (see Janson et al. 2012). This affects the mass ratio distribution in a way that is difficult to quantify. In order to mitigate the third issue, we only consider binaries outside of $1''$ separation (see Fig. 5). This completely avoids the bias, but also leaves us with a smaller sample, such that less stringent conclusions can be drawn about the mass ratio distribution than the semi-major axis distribution.

The procedure for determining the distribution is the same as in the previous section, apart from that we consider $1''$ instead of 100 mas as the effective inner working angle, and obviously that we compare the mass ratio distributions of the real and simulated samples instead of the semi-major axis distribution. We test three cases of mass ratio distributions: a uniform distribution ($f \sim q^0$), a linearly increasing distribution ($f \sim q^1$), and a uniform distribution but with a cut-off at some minimum mass ratio q_{\min} , for which we test a range of values. These different cases are illustrated in Fig. 6. As a semi-major axis distribution, we sim-

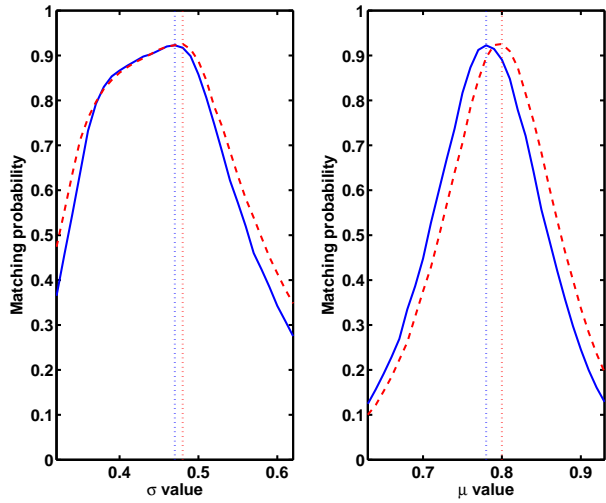


Fig. 4.— Match probabilities from the test in which the μ_a and σ_a parameters of the simulated Gaussian semi-major axis distribution function were varied, and the resulting distribution tested against the measured sample. Blue solid lines represent simulations based on an underlying uniform mass ratio distribution, and red dashed lines represent simulations based on a linearly increasing mass ratio distribution. Left: The distribution of probabilities as function of σ_a , for a cross-section in the parameter grid along $\mu_a = 0.78$ in the uniform case, and along $\mu_a = 0.80$ in the linearly increasing case. Right: The distribution of probabilities as function of μ_a , for a cross-section in the grid along $\sigma_a = 0.47$ in the uniform case, and along $\sigma_a = 0.48$ in the linearly increasing case. Dotted lines denote the location of the global probability maximum in each case. As can be seen, there is a well-defined maximum in each distribution, and the uniform and linearly increasing cases give very similar results, showing that the underlying mass ratio distribution does not significantly affect the determination of the semi-major axis distribution.

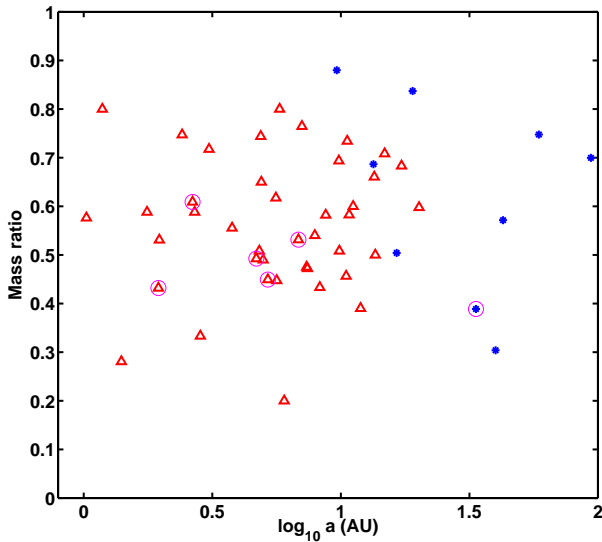


Fig. 5.— Estimated semi-major axis versus mass ratio for the statistically clean sample (see Sect. 6.1). The red triangles are inside of $1''$ projected separation, which makes them unsuitable for assessing a mass ratio distribution due to the false triple bias discussed in the text. Hence, only the blue asterisks are used for this purpose. Binaries for which physical companionship is probable but has not yet been demonstrated through common proper motion are encircled in magenta.

ply choose $\mu_a = 0.78$ and $\sigma_a = 0.47$ here – as with the reverse case, the specific choice of semi-major axis distribution does not affect the results in any significant way. The uncertainties in the measured mass ratios are represented by assigning Gaussian distributed random errors given by the estimated values listed in Table 3 to the mean mass ratios, with a different random seed for each simulation.

We find that a uniform distribution provides a match probability of 58.0%, which is an entirely reasonable fit to the data. However, the distribution is unconstrained at small mass ratios. For instance, a uniform distribution with a cut-off at $q_{\min} = 0.3$ gives a match probability 84.1%, which is an even better fit. We therefore step through q_{\min} in steps of 0.01 in order to test when it becomes marginally inconsistent with the data, which we count here as a match probability of less than $\sim 33\%$, i.e. equivalent to a typical 1σ rejection. This occurs at a q_{\min} of 0.39. A linearly increasing mass ratio gives a match probability of 53.0%. This is almost equally consistent with the data as the fully uniform distribution, underlining the fact that the mass ratio distribution is largely unconstrained.

The range of q_{\min} that fit the data (~ 0.0 –0.39) give a range of possible detectable fractions, which feeds back into the multiplicity fraction discussed in Sect. 6.1. The lowest q_{\min} (fully uniform distribution) gives a detectable fraction of 66.6%, and the highest gives a fraction of 85.4%.

8. Discussion

As we have seen, the mass ratio distribution is one of the main contributors to uncertainty in the total multiplicity fraction. Aside from the caveats already mentioned in the mass ratio determination, it could also be the case that the mass ratio distribution has a dependence on semi-major axis. Such a dependence has been hinted at in several other multiplicity studies (e.g. Janson et al. 2013; Lafrenière et al. 2014). If so, the mass ratio distribution determined at $>1''$ may not be representative for the $<1''$ region where the majority of binaries reside. Nonetheless, it appears that values of ~ 21 –27% appropriately bracket the most plausible total multiplicity fraction range. This range is fully consistent with a smoothly decreasing multiplicity fraction as function of primary mass, as arrived at in many previous studies (e.g. Kouwenhoven et al. 2007; Raghavan et al. 2010; Janson et al. 2012). In Fig. 7,

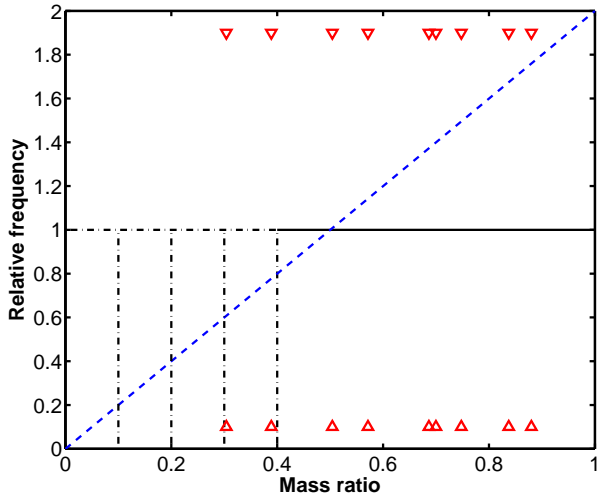


Fig. 6.— Illustration of the various mass ratio distributions used in the simulations. The black lines represent a uniform distribution in mass ratio. The dash-dotted lines represent different possible choices of a lower cut-off in mass ratio q_{\min} . The dashed blue line represents a linearly increasing mass ratio distribution. Each pair of red arrows represents the mass ratio of a binary pair used in the test (most detected pairs in the survey have $<1''$ separations, and are therefore excluded in this analysis). The mass ratio distribution is only loosely constrained, and all of the distributions illustrated here are formally consistent with the observational data.

we show a comparison between the multiplicity fraction of our full sample and the multiplicity as a function of spectral type from Janson et al. (2012). Our derived multiplicity is well consistent with this previous study. The two studies imply a smooth evolution across the M-type range, with no evidence for any sudden jumps, which has been suggested in some scenarios that consider star and brown dwarf formation as separate processes (e.g. Thies & Kroupa 2007).

It is currently not possible to distinguish stringently whether the mass ratio distribution remains close to uniform toward small mass ratios, or whether it starts to decrease somewhere below $q = 0.4$. It is in any case clear that there is no sharp cut-off below a q of ~ 0.8 , as has been reported for the yet lower-mass sample of VLM stars and brown dwarfs (e.g. Burgasser et al. 2007). There could however in principle be such a cut-off in the $q < 0.4$ range, as our analysis with q_{\min} in Sect. 7 demonstrates. If so, the necessarily lower threshold of our sample could imply that there would be some characteristic secondary mass for which companions become less frequent. However, this should obviously be taken as mere speculation at this point, given the incompleteness issues, in addition to the difficulties in the mass ratio determinations.

The semi-major axis distribution, on the other hand, is well constrained by the data, since the AstraLux sensitivity range covers the majority of the range of where the binaries reside, encompassing both sides of a distribution that is well represented by a Gaussian function. As derived in Sect. 6.2 and shown in Fig. 3, a Gaussian distribution with $\mu_a = 0.78$ and $\sigma_a = 0.47$ matches the data at $>90\%$ probability. By contrast, a Sun-like distribution with $\mu_a = 1.64$ and $\sigma_a = 1.52$ (Raghavan et al. 2010) only has a $< 0.03\%$ probability of matching the data and can be firmly excluded. Thus, the result fits the trend of a semi-major axis that gets continuously narrower and closer in with decreasing primary mass (e.g. Burgasser et al. 2007; Janson et al. 2012), with an opposite trend toward higher masses (e.g. Kouwenhoven et al. 2007; Janson et al. 2013).

Most trends observed here and in other studies of low-mass stars are consistent with a smooth transition from the highest-mass stars to the lowest mass brown dwarfs in the field (e.g. Luhman et al. 2005b; Bourke et al. 2006), possibly implying a universal formation scenario for this whole range of objects. The main remaining mystery in this regard is the mass ratio distribution, which appears to be markedly different between stars and brown dwarfs (e.g. Goodwin

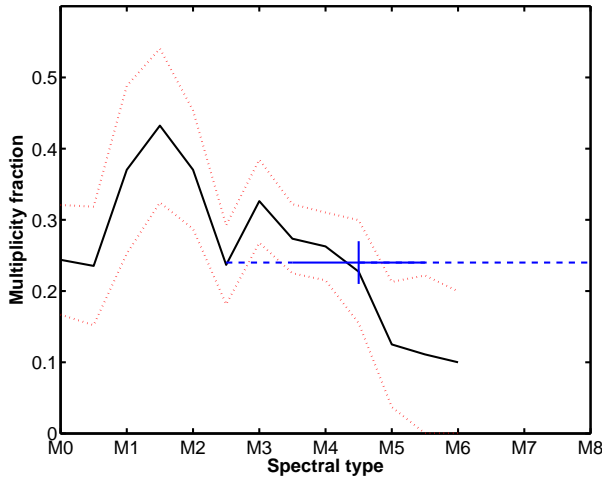


Fig. 7.— Multiplicity fraction of low-mass stars as function of spectral type. The solid black and dotted red lines are multiplicity values (mean and error bars) from Janson et al. (2012). The blue orthogonal lines represent the multiplicity in this sample. The solid horizontal line is the median (M4.5) plus/minus one standard deviation (1 spectral sub-type) for the spectral types in the sample. The dashed line represents the full spectral type range of the sample, excluding I04122+6443 which was classified as M5 in Lépine & Gaidos (2011) but M1 in Bender & Simon (2008). The multiplicity fraction derived here is consistent with the results from Janson et al. (2012).

2013). Given the many difficulties in assigning reliable masses to low-mass objects, however, it would be valuable to further study the mass ratios of both our systems and systems of yet lower mass. We are currently looking into ways in which this could be done. A high-resolution spectrograph with adaptive optics capacity, such as CRIRES at the VLT (Käufl et al. 2004), could measure the individual radial velocities of the components of binaries discovered here, and thus could directly measure model-independent mass ratios over a relatively short timeframe. This would greatly assist studies of multiplicity properties of low-mass stars and brown dwarfs, by aiding in both mass ratio distribution and multiplicity fraction determinations.

9. Conclusions

We have presented observations of 286 mid/late M-dwarfs using the AstraLux Norte camera at Calar Alto in Spain. We resolved 66 probable or confirmed multiple systems, of which 41 were new discoveries. The majority of binary candidates were observed twice or more, and could be confirmed as bona fide companions.

Based on these discoveries and evaluations of the sensitivity range of AstraLux Norte, we deduced a multiplicity fraction inside of the AstraLux sensitivity range of 17.9%, corresponding to a total multiplicity fraction of 21–27%. The mass ratio distribution is consistent with being uniform down to $q = 0.4$, but cannot be stringently constrained below this value. The semi-major axis distribution is well represented by a Gaussian function with $\mu_a = 0.78$ and $\sigma_a = 0.47$ – a function which is significantly narrower and peaked at smaller separations than the corresponding distribution of Sun-like stars.

Most observables point to continuous distributions and a common formation scenario for stars and brown dwarfs, but some discrepancies persist, most notably in the mass ratio distribution. This is however also one of the most uncertain distributions, and more work will be required in the future to more robustly assess mass ratios at the low-mass tail of the stellar population.

We thank all the staff at the Calar Alto observatory for their support. This study made use of the CDS services SIMBAD, VizieR, and CDS Portal, as well as the SAO/NASA ADS service. Some of the archival study was based on photographic data of the National Geographic Society – Palomar Observatory Sky Survey

(NGS-POSS) obtained using the Oschin Telescope on Palomar Mountain. The NGS-POSS was funded by a grant from the National Geographic Society to the California Institute of Technology. The plates were processed into the present compressed digital form with their permission. The Digitized Sky Survey was produced at the Space Telescope Science Institute under US Government grant NAG W-2166. Other parts of the archival study make use of data products from the Two Micron All Sky Survey, which is a joint project of the University of Massachusetts and the Infrared Processing and Analysis Center/California Institute of Technology, funded by the National Aeronautics and Space Administration and the National Science Foundation.

REFERENCES

- Agüeros, M.A., Anderson, S.F., Covey, K.R. et al. 2009, *ApJS* 181, 444
- Alcalá, J.M., Covino, E., Torres, G., Sterzik, M.F., Pfeiffer, M.J., & Neuhäuser, R. 2000, *A&A* 353, 186
- Allard, F., Hauschildt, P., Alexander, D.R., Tamai, A., & Schweitzer, A. 2001, *ApJ* 556, 357
- Allard, F. 2014, *IAUS* 299, 271
- Babu, G.J. & Feigelson, E.D. 2006, in *ASP Conf. Ser. 351, Astronomical Data Analysis Software and Systems XV*, ed. C. Gabriel, C. Arviset, D. Ponz, & S. Enrique (San Francisco, CA: ASP), 127
- Baraffe, I., Chabrier, G., Allard, F., & Hauschildt, P.H. 1998, *A&A* 337, 403
- Baraffe, I., Chabrier, G., Barman, T.S., Allard, F., & Hauschildt, P.H. 2003, *A&A* 402, 701
- Bate, M.R. 2012, *MNRAS* 419, 3115
- Bender, C.F. & Simon, M. 2008, *ApJ* 689, 416
- Benedict, G.F., McArthur, B.E., Franz, O.G., Wasserman, L.H., & Henry, T.J. 2000, *AJ* 120, 1106
- Bergfors, C. et al. 2010, *A&A* 520, 54
- Bergfors, C. et al. 2013, *MNRAS* 428, 182
- Beuzit, J.-L. et al. 2004, *A&A* 425, 997
- Binks, A.S. & Jeffries, R.D. 2014, *MNRAS* 438, L11
- Bonfils, X. et al. 2013, *A&A* 549, 109
- Bourke, T.L. et al. 2006, *ApJ* 649, L37
- Brandeker, A., Jayawardhana, R., Khavari, P., Haisch, K.E., & Mardones, D. 2006, *ApJ* 652, 1572
- Burgasser, A., Reid, I.N., Siegler, N., Close, L., Allen, P., Lowrance, P., & Gizis, J. 2007, in *Protostars and Planets V*, ed. B. Reipurth, D. Jewitt & K. Kiel, 427
- Burrows, A., Hubbard, W.B., Saumon, D., & Lunine, J.I. 1993, *ApJ* 406, 158
- Burrows, A. et al. 1997, *ApJ* 491, 856
- Caballero, J.A. 2007, *ApJ* 667, 520
- Caballero, J.A., Montes, D., Klutsch, A., Genebriera, J., Miret, F.X., Tobal, T., Cairol, J., & Pedraz, S. 2010, *A&A* 520, 91
- Close, L.M., Siegler, N., Freed, M., & Biller, B. 2003, *ApJ* 587, 407
- Costa, E., Méndez, R.A., Jao, W.-C., Henry, T.J., Subsavage, J.P., Brown, M.A., Ianna, P.A., & Bartlett, J. 2005, *AJ* 130, 337
- Daemgen, S., Siegler, N., Reid, I.N., & Close, L.M. 2007, *ApJ* 654, 558
- Daemgen, S., Hormuth, F., Brandner, W., Bergfors, C., Janson, M., Hippler, S., & Henning, T. 2009, *A&A* 498, 567
- Delfosse, X., Forveille, T., Perrier, C., & Mayor, M. 1998, *A&A* 331, 581
- Delfosse, X., Forveille, T., Mayor, M., Burnet, M., & Perrier, C. 1999, *A&A* 341, L63
- Delfosse, X. et al. 2004, in *Spectroscopically and Spatially Resolving the Components of Close Binary Stars*, ed. R.W. Hilditch, H. Hensberge & K. Pavlovski, *ASP Conf. Ser.* 318, 166
- Dittmann, J.A., Irwin, J.M., Charbonneau, D., & Berta-Thompson, Z.K. 2014, *ApJ* 784, 156
- Duchêne, G. & Kraus, A. 2013, *ARA&A* 51, 269
- Dupuy, T.J., Liu, M.C., Bowler, B.P., Cushing, M.C., Helling, C., Witte, S., & Hauschildt, P. 2010, *ApJ* 721, 1725
- Duquennoy, A. & Mayor, M. 1991, *A&A* 248, 485

- Faherty, J.,K., Burgasser, A.J., Cruz, K.L., Shara, M.M., Walter, F.M., & Gelino, C.R. 2009, AJ 137, 1
- Fischer, D. & Marcy, G. 1992, ApJ 396, 178
- Gatewood, G. 2008, AJ 136, 452
- Gatewood, G. & Coban, L. 2009, AJ 137, 402
- Gigoyan, K.S. & Mickaelian, A.M. 2012, MNRAS 419, 3346
- Gliese, W. & Jahreiss, H. 1991, Third Catalogue of Nearby Stars, <http://cdsarc.u-strasbg.fr/viz-bin/Cat?V/70A>
- Goodwin, S.P. & Kroupa, P. 2005, A&A 439, 565
- Goodwin, S.P. 2013, MNRAS 430, 6
- Harrington, R.S., Christy, J.W., & Strand, K.A. 1981, AJ 86, 909
- Harrington, R.S., Dahn, C.C., Kallarakal, V.V. et al. 1993, AJ 105, 1571
- Hartkopf, W.I., Tokovinin, A., & Mason, B.D. 2012, AJ 143, 42
- Hartman, J.D., Bakos, G.Á., Noyes, R.W., Sipocz, B., Kovács, G., Mazeh, T., Shporer, A., & Pál, A. 2011, AJ 141, 166
- Hauschildt, P., Allard, F., Ferguson, J., Baron, E., & Alexander, D.R. 1999, ApJ 525, 871
- Henry, T.J., Ianna, P.A., Kirkpatrick, J.D., & Jahreiss, H. 1997, AJ 114, 388
- Henry, T.J., Jao, W.-C., Subsavage, J.P., Beaulieu, T.D., Ianna, P.A., Costa, E., Méndez, R.A. 2006, AJ 132, 2360
- Hippler, S. et al. 2009, The Messenger 137, 14
- Horch, E.P., Bahi, L.A.P., Gaulin, J.R., Howell, S.B., Sherry, W.H., Baena Gallé, R., & van Altena, W.F. 2012, AJ 143, 10
- Hormuth, F., 2007, Diploma Thesis, Univ. of Heidelberg
- Hormuth, F., Brandner, W., Hippler, S., Janson, M., & Henning, T. 2007, A&A 463, 707
- Hormuth, F., Hippler, S., Brandner, W., Wagner, K., & Henning, T. 2008, SPIE 7104, 138
- Ireland, M.J., Kraus, A., Martinache, F., Lloyd, J.P., & Tuthill, P.G. 2008, ApJ 678, 463
- Irwin, J. et al. 2009, ApJ 701, 1436
- Janson, M., Brandner, W., Lenzen, R., Close, L., Nielsen, E., Hartung, M., Henning, T., Bouy, H. 2007, A&A 462, 615
- Janson, M., Bonavita, M., Klahr, H., Lafrenière, D., Jayawardhana, R., & Zinnecker, H. 2011, ApJ 736, 89
- Janson, M., Hormuth, F., Bergfors, C., et al. 2012, ApJ 754, 44
- Janson, M., Lafrenière, D., Jayawardhana, R., Bonavita, M., Girard, J., Brandeker, A., & Gizis, J.E. 2013, ApJ 773, 170
- Jao, W.-C., Henry, T.J., Subsavage, J.P., Winters, J.G., Gies, D.R., Riedel, A.R., Ianna, P.A. 2014, AJ 147, 21
- Jenkins, J.S., Jones, H.R.A., Goźdiewski, K. 2009, MNRAS 398, 911
- Jódar, E., Pérez-Garrido, A., Díaz-Sánchez, A., Villó, I., Rebolo, R., & Pérez-Prieto, J.A. 2013, MNRAS 429, 859
- Käufl, H.U. et al. 2002, Proc. SPIE 5492, 1218
- Khrutskaya, E.V., Izmailov, I.S., & Khovrichev, M.Y. 2010, Astron. Lett. 36, 576
- Köhler, R., Ratzka, T., Herbst, T.M., & Kasper, M. 2008, A&A 482, 929
- Kouwenhoven, M.B.N., Brown, A.G.A., Portegies Zwart, S.F., & Kaper, L. 2007, A&A 474, 77
- Lafrenière, D., Doyon, R., Marois, C. et al. 2007, ApJ 670, 1367
- Lafrenière, D., Jayawardhana, R., van Kerkwijk, M.H., Brandeker, A., & Janson, M. 2014, ApJ 785, 47
- Law, N.M., Hodgkin, S.T., & Mackay, C.D. 2006, MNRAS 368, 1917
- Law, N.M. 2006, Ph.D. thesis, Institute of Astronomy & Selwyn College, Cambridge University
- Law, N.M., Hodgkin, S.T., & Mackay, C.D. 2008, MNRAS 384, 150

- Lépine, S. 2005, AJ 130, 1680
- Lépine, S., Thorstensen, J.R., Shara, M.M., & Rich, R.M. 2009, AJ 137, 4109
- Lépine, S. & Gaidos, E. 2011, AJ 142, 138
- Lippincott, S.L. 1975, AJ 80, 831
- Luhman, K.L., Stauffer, J.R., & Mamajek, E.E. 2005, ApJ 628, L69
- Luhman, K.L. et al. 2005, ApJ 631, 69
- Malo, L., Doyon, R., Lafrenière, D., Artigau, E., Gagné, J., Baron, F., & Riedel, A. 2013, ApJ 762, 88
- Mann, A.W., Brewer, J.M., Gaidos, E., Lépine, S., & Hilton, E.J. 2013, AJ 145, 52
- Marks, M. & Kroupa, P. 2011, MNRAS 417, 1702
- Martinache, F., Rojas-Ayala, B., Ireland, M.J., Lloyd, J.P., & Tuthill, P.G. 2009, ApJ 695, 1183
- Mason, B.D., Wycoff, G.L., Hartkopf, W.I., Douglass, G.G., & Worley, C.E. 2001, AJ 122, 3466
- McCarthy, C., Zuckerman, B., & Becklin, E.E. 2001, AJ 121, 3259
- McCaughrean, M.J. & Stauffer, J.R. 1994, AJ 108, 1382
- Mochnacki, S.W. et al. 2002, AJ 124, 2868
- Mohanty, S. & Basri, G. 2003, ApJ 583, 451
- Monet, D.G., Dahn, C.C., Vrba, F.J., Harris, H.C., Pier, J.R., Luginbuhl, C.B., & Ables, H.D. 1992, AJ 103, 638
- Montagnier, G. et al. 2006, A&A 460, L19
- Motch, C., Guillout, P., Haberl, F. 1998, A&AS 132, 341
- Perryman, M.A.C. et al. 1997, A&A 323, 49
- Peter, D., Feldt, M., Henning, T., & Hormuth, F. 2012, A&A 538, 74
- Pourbaix, D. 2000, A&AS 145, 215
- Pravdo, S.H., Shaklan, S.B., Henry, T., & Benedict, G.F. 2004, ApJ 617, 1323
- Pravdo, S.H., Shaklan, S.B., Wiktorowicz, S.J., Kulka-rni, S., Lloyd, J.P., Martinache, F., Tuthill, P.G., & Ireland, M.J. 2006, ApJ 649, 389
- Prosser, C.F., Stauffer, J., & Kraft, R.P. 1991, AJ 101, 1361
- Raghavan, D. et al. 2010, ApJS 190, 1
- Reggiani, M. & Meyer, M.R. 2013, A&A 553, 124
- Reid, I.N., Hawley, S.L., & Gizis, J.E. 1995, AJ 110, 1838
- Reid, I.N., Cruz, K.L., Allen, P. et al. 2003, AJ 126, 3007
- Reid, I.N., Cruz, K.L., Allen, P. et al. 2004, AJ 128, 463
- Reid, I.N., Cruz, K.L., & Allen, P.R. 2007, AJ 133, 2825
- Riedel, A.R., Subsavage, J.P., Finch, C.T. et al. 2010, AJ 140, 897
- Reidel, A.R. et al. 2014, AJ 147, 85
- Reipurth, B., Boss, A.P., Clarke, C., Goodwin, S.P., Rodriguez, L.F., Stassun, K.G., Tokovinin, A., & Zinnecker, H. 2014, Proc. PPVI, accepted
- Riaz, B., Gizis, J., & Harvin, J. 2006, AJ 132, 866
- Saumon, D. & Marley, M.S. 2008, ApJ 689, 1327
- Schlieder, J.E., Lépine, S., Rice, E., Simon, M., Fielding, D., & Tomasino, R. 2012, AJ 143, 114
- Schlieder, J.E., Lépine, S., & Simon, M. 2012, AJ 144, 109
- Schlieder, J.E. et al. 2014, ApJ 783, 27
- Scholz, R.-D., Meusinger, H., Jahreiss, H. 2005, A&A 442, 211
- Shkolnik, E., Liu, M.C., & Reid, I.N. 2009, ApJ 699, 649
- Shkolnik, E., Hebb, L., Liu, M., Reid, N., & Cameron, A.C. 2010, ApJ 716, 1522
- Shkolnik, E., Anglada-Escudé, G., Liu, M.C., Bowler, B.P., Weinberger, A.J., Boss, A.P., Reid, I.N., & Tamura, M. 2012, ApJ 758, 56
- Skrutskie, M.F. et al. 2006, AJ 131, 1163

Thies, I. & Kroupa. P. 2007, ApJ 671, 767

Tubbs, R.N., Baldwin, J.E., Mackay, C.D., & Cox, G.C. 2002, A&A 387, 21

van Altena, W.F., Lee, J.T., & Hoffleit, E.D. 1995, The general catalog of trigonometric stellar parallaxes, eds. W.F van Altena, J.T. Lee & E.D. Hoffleit

van der Marel, R.P., Gerssen, J., Guhathakurta, P., Peterson, R.C., & Gebhardt, K. 2002, AJ 124, 3255

van Leeuwen, F. 2007, A&A 474, 653

Zuckerman, B., Song, I., Bessell, M.S. & Webb, R.A. 2001, ApJ 562, L87

A. Notes on individual targets

In this section, we list special remarks on individual targets, where relevant.

I00235+7711 (GJ 1010) As noted in the Washington Double Star (WDS) catalogue (e.g. Mason et al. 2001), this star is a member of an 11'' binary. Both components are visible in full-frame AstraLux images, but since the separation is larger than the region of completeness, I00235+7711 counts as a single star within this range.

I00395+1454N (G 32-37 B) As implied by its identifier, I00395+1454N has a wide binary companion toward the south at a separation of 17'' according to the WDS, which is not included in the AstraLux field of view. Given the new detection of a closer companion with AstraLux, it is probable that the system is in reality at least a triple system.

I00413+5550W (GJ 1015 A) I00413+5550W has a 10'' companion to the East that is noted in WDS. It is visible in the AstraLux image but outside of its completeness range, and thus the star counts as single for statistical purposes.

I01028+4703 (G 172-35) This target is a component of a 15'' binary noted in WDS, which is visible in the AstraLux images, but outside of the completeness range.

I01076+2257E (GJ 9040 B) As its name implies, I01076+2257E is a secondary component in a 10'' binary noted in WDS, which can be seen in the AstraLux images, but does not count in our analysis due to its >5'' separation.

I02027+1334 (GJ 3129) This target has been noted as a double-lined spectroscopic binary with an estimated maximum semi-major axis of 0.13 AU (Shkolnik et al. 2010). As expected, it is therefore not detected in AstraLux imaging. There are no other companions seen with AstraLux, and it thus counts as single in the statistics.

I03325+2843 (J03323578+2843554) This triple system has been observed in several epochs, as reported in Janson et al. (2012). We will discuss it in more detail in a near-future study (Janson et al., in prep.) that analyzes systems observed in multiple epochs with AstraLux. The BC pair doesn't count as a separate pair in the statistical analysis, since its separation is just below 100 mas in the epoch considered here. The measured brightness differences between the B and C components are $\Delta z' = 0.58 \pm 0.12$ mag and $\Delta i' = 1.03 \pm 0.08$ mag.

I03372+6910 (GJ 3236) The I03372+6910 system is a known double-lined spectroscopic binary (Shkolnik et al. 2010), which is also eclipsing (Irwin et al. 2009), and thus is of significant use for calibration of low-mass stellar properties. The companion is at a <0.1 AU separation and thus beyond the AstraLux sensitivity range, where we find no additional companions.

I03392+5632 (G 175-2) In addition to the companion discovered in this study, there is a known wide (24'') common proper motion companion noted in WDS, hence the system is at least triple in reality.

I04123+1615 (LP 414-117) There is a spectroscopic binary companion to this star with an orbital period of ~ 128 days (Bender & Simon 2008). It is too close to be spatially resolved with AstraLux, and there are no other companions within the sensitivity range of our study.

I04129+5236 (LHS 1642) I04129+5236 is a known close binary system with a well-determined orbit (Pravdo et al. 2004; Martinache et al. 2009). Its separation is smaller than 100 mas at all times, and it therefore remains unresolved by AstraLux. We do detect one other point source in the field of view, but it is a suspected background contaminant based on its blue color, with $\Delta z' = 5.8 \pm 0.1$ mag and $\Delta i' = 5.3 \pm 0.1$ mag.

I04247-0647 (**J04244260-0647313**) This is a target that overlaps with our previous study in Janson et al. (2012). As we already noted there, it is single in the AstraLux field of view, but it is a triple-lined spectroscopic multiple system further in Shkolnik et al. (2010).

I04308-0849S (Koenigstuhl 2 B) Another target that overlaps with Janson et al. (2012), this star is single in the AstraLux field but has a known wide common proper motion companion at 17'' separation (Caballero 2007).

I04388+2147 (G 8-48) In addition to the companion discovered here, there is a wide binary companion at 15'' separation noted in the WDS, hence it is likely that the system is at least a triple.

I04425+2027 (J04423029+2027115) This is a double-lined spectroscopic binary with a period of a few days (Mochnacki et al. 2002), which is far too close to be resolved with AstraLux. It is single in our sensitivity range.

I05030+2122 (LP 359-186) For binaries with a small brightness difference between the components, one should always be wary of potential 180° phase shifts between different astrometric epochs. For this system, such a shift in the Law et al. (2008) data point with respect to our two epochs seems highly probable, given the consistency in apparent

orbital motion when such a shift is considered ($\sim 1^\circ$ per year in each case with the shift included, versus a sudden change from $\sim 30^\circ$ per year to $\sim 1^\circ$ per year when it is not). The quoted value in Table 2 therefore includes such a shift.

I06171+0507 (NLTT 16333) I06171+0507 is a close binary that has been previously resolved in several epochs by Pravdo et al. (2006), and which we re-detect with AstraLux. The pair is itself part of a higher-order multiple system with the bright star HR 2251 at a $103''$ separation.

I06579+6219 (GJ 3417, LHS 1885) If taken at face value, the body of astrometric points that exists for this target does not make sense. Three epochs of astrometry exists: One from Henry et al. (1997) taken in 1996 ($\rho = 2.0''$ and $\theta = 220^\circ$), one from Law et al. (2008) taken in 2005 ($\rho = 1.5''$ and $\theta = 320^\circ$), and our data point taken in 2012 ($\rho = 1.4''$ and $\theta = 240^\circ$). Given that background objects can be firmly excluded, this would imply an enormously fast orbital motion since the binary would move from 220° to 320° and then back to 240° within 16 years, which is impossible for such a low-mass binary with a ~ 17 AU semi-major axis. However, the astrometry becomes entirely sensible in an orbital motion framework if we impose a 90° phase shift on the Law et al. (2008) position angle such that it is 230° instead, giving a continuous motion of 20° in 16 years. In Janson et al. (2012), we suggested an equal phase shift for similar reasons for the Law et al. (2008) data point in the J15553178+3512028 binary system. We thus include such a shift in Table 2.

I07111+4329 (J07111138+4329590) I07111+4329 is a known binary that has been observed previously over several epochs (e.g. Dupuy et al. 2010). There is also a background star in the field of view, with $\Delta z' = 5.7 \pm 0.1$ mag and $\Delta i' = 4.2 \pm 0.1$ mag.

I07307+4811 (LHS 229) Although this star looks single in the AstraLux images, it is in fact part of a quadruple system (Harrington et al. 1981). I07307+4811 itself is a close binary M-dwarf pair with a separation of ~ 50 mas, too close to be resolved here. In addition, at a $103''$ separation far beyond the AstraLux field of view, there is a pair of white dwarfs that are physically bound to this system.

I07320+1719W (G 88-35) As implied by its identifier, I07320+1719W is part of a wide binary system registered in WDS with an $11''$ separation. It is visible in the AstraLux images, but beyond the completeness range of the instrument.

I08119+0846 (LHS 35) There is a relatively strong linear trend noted in the radial velocity analysis for the target in Bonfils et al. (2013). Such trends can be signs of stellar companions, but in this case we detect no companions in the AstraLux data.

I08316+1923 (CU Cnc and CV Cnc) This is a known quintuple system, as reported in e.g Delfosse et al. (1999) and Beuzit et al. (2004). Four of the components are resolved in two separate pairs (AaAb and BaBb) by AstraLux. The two pairs themselves (CU Cnc and CV Cnc) are too far separated for the AstraLux completeness range, and so they count as two separate binary pairs for statistical purposes. The fifth component is unresolved in the images; this is an eclipsing binary companion to the Aa component.

I08589+0828 (G 41-14) I08589+0828 is a triple system with a close spectroscopic pair on a 7.6 day orbit, and one wider component which is reported at a separation of 620 mas in Delfosse et al. (1999). Subsequently, an orbit has been determined for the wider pair (Hartkopf et al. 2012), with a period of 5.66 years and a 424 mas angular semi-major axis. Using the estimated orbital elements to predict the location of the wider component in Jan 2012 when the AstraLux image was taken, the predicted separation is ~ 100 mas. This is in excellent agreement with what is seen in the AstraLux image, where the PSF is substantially extended, but not quite sufficiently to get a satisfactory binary fit. Since the fit does not converge, the star counts as single within the AstraLux sensitivity range.

I10497+3532 (GJ 1138) I10497+3532 has been previously reported as a 300 mas binary Beuzit et al. (2004). The fact that it looks single in our AstraLux images despite the excellent quality of those observations implies that it must have undergone substantial orbital motion, bringing it to a much smaller (< 100 mas) projected separation in June of 2012. The non-detectability in AstraLux images means that it counts as a single system for the purpose of the multiplicity analysis performed here.

I13143+1320 (NLTT 33370) Recently, Schlieder et al. (2014) reported I13143+1320 as a binary. In NACO images that are approximately coincident with the AstraLux images, the projected separation of the binary is ~ 75 mas, which

is consistent with the fact that the binary is unresolved in the AstraLux images. It counts as a single system in the analysis performed here.

I15474+4507 (G 179-55) This star is a known eclipsing and double-lined spectroscopic binary with a period of 3.55 days (Hartman et al. 2011). The separation is far too small to be resolved with AstraLux, and we detect no other companions within the AstraLux field of view.

I16555-0823 (GJ 644 C) While the star I16555-0823 (also known as VB 8) itself is single in the AstraLux sensitivity range, it is part of a higher-order multiple (at least triple, possibly quintuple) as a known 1500 AU companion to GJ 644, which was discussed in our Janson et al. (2012) study.

I18180+3846W (LHS 461) I18180+3846W has a 10'' companion to the East registered in WDS. It is visible in the AstraLux images, but outside of the completeness range. There are no other candidates observed in the field.

I18427+1354 (GJ 4071) There is a point source at 3.7'' separation from I18427+1354. The system has only been observed in one epoch, but based on the colors of the candidate ($\Delta z' = 5.8 \pm 0.1$ mag and $\Delta i' = 5.7 \pm 0.1$ mag), it counts as a probable background contaminant in our analysis.

I19312+3607 (G 125-15) While I19312+3607 has no candidates visible in the AstraLux images, it is actually a triple system. I19312+3607 itself is noted as a very close (<0.01 AU) double-lined spectroscopic binary in Shkolnik et al. (2010). Additionally, there is a wide common proper motion companion at 46'' citepcaballero2010.

I20298+0941 (HU Del) The I20298+0941 system is a well known astrometric binary (e.g. Benedict et al. 2000), but to our knowledge, the AstraLux images represent the first instance in which the binary has been spatially resolved.

I20433+5520 (GJ 802 A) I20433+5520 is a well-studied close triple system (e.g. Ireland et al. 2008). It consists of a spectroscopic pair with a period of only 19 h, and a brown dwarf at a separation of ~ 90 mas. Both are too close to be resolved with AstraLux, and there are no other candidates in the field of view.

I21000+4004E (GJ 815 A) In addition to the component that we resolve with AstraLux, which was previously known and has been studied over a long timescale (e.g. Lippincott 1975), the primary component of the resolved pair is a 3.3 day spectroscopic binary (Pourbaix 2000),

I21109+4657S (G 212-27) Both of the point sources in the AstraLux field of view are consistent with static background objects that do not share a common proper motion with the primary star, hence they are contaminants rather than physical companions. Their colors ($\Delta z' = 4.0 \pm 0.3$ mag and $\Delta i' = 3.3 \pm 0.5$ mag for the closer point source and $\Delta z' = 4.8 \pm 0.3$ mag and $\Delta i' = 4.3 \pm 0.1$ mag for the farther one) verify this conclusion.

I21160+2951E (GJ 4185 A) Although I21160+2951E is single within the AstraLux field of view, it has a wide companion at 26'' separation. It also appears that I21160+2951E is itself a close binary pair; this is implied in Shkolnik et al. (2012), but an as of yet unpublished paper is referred to for the specific properties of this pair. Since a general comment is made that separations down to 40 mas are being probed, it is presumably the case that the third component of the system is simply too close in to be resolved with AstraLux.

I21376+0137 (J21374019+0137137) This newly discovered binary candidate is a probable member of the β Pic moving group according to the Schlieder et al. (2012b) study. Its relatively small projected separation of ~ 4.5 AU implies that its orbit could be dynamically constrained in a reasonable timeframe, which makes it a potential benchmark binary in the future.

I23318+1956E (EQ Peg B) This wide binary used to have a separation that would have kept it inside of the completeness range of AstraLux (e.g., 3.5'' separation in 1941 according to WDS), but at the AstraLux epoch it is just outside of this range, at 5.4''. It therefore counts as being outside of this range.

Table 1:: General properties of all targets observed in the survey.

Lepine ID	α (hh mm ss)	δ (dd mm ss)	PM_α (mas)	PM_δ (mas)	π (mas)	e_π (mas)	Ref ^a	Spt ^b	Ref ^c	J (mag)	Mult ^d	ND ^e
I00066-0705	00 06 39.249	-07 05 35.33	-104	89	69.9	21.0	PHOT	M3.5	R07	9.83	M	N
I00077+6022	00 07 42.620	+60 22 54.34	340	-27	68.6	2.0	D14	M3.8	Sh09	8.91	M	Y
I00088+2050	00 08 53.922	+20 50 25.45	-65	-247	67.5	2.7	D14	M4.5	R95	8.87	M	N
I00115+5908	00 11 31.808	+59 08 39.87	-918	-1164	108.3	1.4	L09	M6.5	L09	9.94	S	—
I00132+6919N	00 13 15.850	+69 19 37.62	717	-292	49.9	6.0	vL07	M3.0	R95	8.56	M	N
I00162+1951E	00 16 16.142	+19 51 50.61	704	-740	66.1	1.6	vA95	M4.0	R95	8.89	S	—
I00169+0507	00 16 56.298	+05 07 26.54	-107	-629	56.9	3.7	vA95	M4.5	R95	9.40	S	—

Table 1:: continued.

Lepine ID	α (hh mm ss)	δ (dd mm ss)	PM_α (mas)	PM_δ (mas)	π (mas)	e_π (mas)	Ref ^a	Spt ^b	Ref ^c	J (mag)	Mult ^d	ND ^e
I00235+7711	00 23 31.836	+77 11 26.73	-848	26	52.0	2.0	vL07	M4.0	R95	9.93	O	—
I00253+2253	00 25 20.599	+22 53 11.10	-245	-450	70.4	3.2	D14	M4.0	R95	9.72	S	—
I00271+4941	00 27 06.783	+49 41 52.88	366	-228	46.9	3.1	vA95	M4.5	R95	9.73	S	—
I00297+0112	00 29 43.207	+01 12 38.69	-159	-133	176.9	53.1	PHOT	m8.0	L11	9.15	S	—
I00313+0009	00 31 21.548	+00 09 29.40	519	103	39.8	2.1	D14	m5.0	L11	9.76	S	—
I00346+7111	00 34 37.657	+71 11 42.11	525	-338	50.7	3.1	vA95	M3.5	R95	9.47	S	—
I00395+1454N	00 39 33.799	+14 54 34.92	315	47	35.3	1.8	vA95	M5.0	L11	9.83	M,W	Y
I00413+5550W	00 41 20.824	+55 50 04.39	325	-70	43.4	2.0	vA95	M4.0	R95	9.84	O	—
I00443+0907	00 44 20.654	+09 07 34.59	821	10	81.0	12.0	G91	M4.5	R95	9.50	S	—
I00464+5038	00 46 29.952	+50 38 38.72	421	-219	57.5	17.2	PHOT	M3.5	R04	9.96	S	—
I00489+4435	00 48 58.236	+44 35 08.96	113	-132	54.0	11.0	G91	M3.0	R95	9.12	M	N
I00502+0837	00 50 17.525	+08 37 34.13	44	-28	66.9	20.1	PHOT	m5.0	L11	9.74	S	—
I00580+3919	00 58 01.157	+39 19 11.18	-112	25	80.5	24.2	PHOT	m5.0	L11	9.56	S	—
I01019+5410	01 01 59.491	+54 10 57.68	-309	-109	91.8	2.8	D14	M5.0	R95	9.78	S	—
I01028+1856	01 02 50.993	+18 56 54.25	94	-53	72.5	21.8	PHOT	M4.0	R06	9.51	S	—
I01028+4703	01 02 53.474	+47 03 02.96	388	-186	31.0	11.0	R04	m5.0	L11	9.35	O	—
I01032+7113	01 03 14.452	+71 13 12.72	506	-65	54.4	2.6	D14	m5.0	L11	9.69	M	Y
I01033+6221	01 03 19.823	+62 21 55.79	737	87	95.5	7.3	vA95	M5.0	R95	8.61	S	—
I01056+2829	01 05 37.636	+28 29 33.57	1903	-189	79.3	3.0	vA95	M5.0	R95	9.49	S	—
I01069+8027	01 06 54.684	+80 27 34.46	203	-24	65.3	4.3	D14	m5.0	L11	9.35	S	—
I01076+2257E	01 07 38.533	+22 57 20.76	102	-492	52.0	8.7	vA95	M3.9	M13	9.53	O	—
I01114+1526	01 11 25.408	+15 26 21.92	186	-120	58.0	7.3	D14	M5.0	R95	9.08	M	N
I01198+8409	01 19 52.149	+84 09 32.88	-986	469	71.6	2.7	vA95	M5.0	R95	9.85	S	—
I01402+3147	01 40 16.569	+31 47 30.66	460	1	53.4	2.1	D14	M4.0	R95	9.44	S	—
I01431+2101	01 43 11.861	+21 01 10.64	-88	5	83.3	25.0	PHOT	m5.0	L11	9.25	M	Y
I01510-0607	01 51 04.050	-06 07 04.76	545	-260	100.8	1.9	H06	M4.5	R95	9.41	S	—
I01514+2123	01 51 24.173	+21 23 39.48	-1	-345	56.3	3.7	D14	M4.0	R95	9.49	S	—
I01562+0006	01 56 14.920	+00 06 08.88	111	-78	79.2	23.7	PHOT	m5.0	L11	9.49	S	—
I01572-0750	01 57 13.227	-07 50 10.98	141	-15	110.8	33.3	PHOT	m7.0	L11	9.80	S	—
I02001+3639	02 00 07.417	+36 39 48.07	54	-264	45.3	1.3	D14	M3.5	R95	9.81	S	—
I02002+1303	02 00 12.965	+13 03 07.07	1091	-1780	224.8	2.9	vA95	M4.5	R95	7.51	S	—
I02007-1021	02 00 47.260	-10 21 20.98	-379	-354	42.0	8.0	G91	M3.5	R95	9.89	S	—
I02019+7332	02 01 54.060	+73 32 31.91	275	-110	87.5	0.6	G09	M4.5	R03	9.25	M	Y
I02022+1020	02 02 16.243	+10 20 13.90	-686	-274	112.0	3.2	vA95	M6.0	R95	9.84	O	—
I02023+0115	02 02 22.381	+01 15 42.80	-79	176	53.4	16.0	PHOT	m5.0	L11	9.81	S	—
I02027+1334	02 02 44.348	+13 34 33.45	454	-103	41.4	6.1	D14	M4.5	R95	9.65	C	—
I02071+6417	02 07 10.333	+64 17 11.45	222	-169	56.7	1.6	D14	M4.0	R95	9.88	S	—
I02129+0000E	02 12 54.622	+00 00 16.79	552	43	65.3	2.1	R10	M4.0	R95	9.06	S	—
I02133+3648	02 13 20.628	+36 48 50.75	24	47	67.9	20.4	PHOT	M4.5	R06	9.37	M	N
I02155+3357	02 15 34.411	+33 57 41.06	168	-371	58.0	11.0	G91	M3.5	R95	9.32	S	—
I02164+1335	02 16 29.853	+13 35 12.66	485	-425	117.7	4.0	vA95	M5.5	R95	9.87	S	—
I02171+3526	02 17 10.023	+35 26 32.47	545	-260	96.4	1.2	M92	M5.0	J09	9.98	S	—
I02274+0310	02 27 27.569	+03 10 54.82	-125	-12	53.5	16.1	PHOT	m5.0	L11	9.98	S	—
I02337+1500E	02 33 47.483	+15 00 17.38	436	36	43.7	2.0	D14	M3.0	R95	9.69	S	—
I02530+1652	02 53 00.886	+16 52 52.69	3386	-3747	259.2	0.9	G09	M7.0	F09	8.39	S	—
I02562+2359	02 56 13.966	+23 59 10.16	67	-163	256.8	8.0	D14	M4.5	R07	9.98	M	Y
I03090+1001	03 09 00.160	+10 01 25.74	270	-571	83.9	4.0	vA95	M5.0	R95	9.93	S	—
I03109+7346	03 10 58.286	+73 46 19.73	1832	-1086	83.3	3.4	vA95	M5.0	R95	9.85	S	—
I03133+0446S	03 13 22.917	+04 46 29.31	1740	93	117.1	3.5	vA95	M5.0	R95	8.77	S	—
I03194+6156	03 19 28.761	+61 56 04.38	222	-192	35.8	3.0	D14	M4.1	Sh09	9.51	M	Y
I03236+0541	03 23 39.163	+05 41 15.32	73	-59	60.7	18.2	PHOT	m5.0	L11	9.87	S	—
I03257+0551	03 25 42.253	+05 51 51.92	-181	-147	43.4	3.5	vA95	M4.5	R95	9.95	M	Y
I03263+1709	03 26 23.628	+17 09 30.91	80	-60	54.7	16.4	PHOT	m5.0	L11	9.77	M	Y
I03309+7041S	03 30 54.809	+70 41 14.09	371	-487	44.7	1.8	D14	m5.0	L11	9.49	M	Y
I03325+2843	03 32 35.795	+28 43 55.36	44	-64	67.3	20.2	PHOT	M4.0	R06	9.36	M	N
I03361+3118	03 36 08.698	+31 18 39.55	114	-123	79.6	2.5	L09	M4.5	R06	9.19	S	—
I03366+0329	03 36 40.832	+03 29 19.57	119	-116	70.0	10.0	G91	M4.5	R95	9.30	S	—
I03372+6910	03 37 14.082	+69 10 49.79	139	-129	27.7	1.3	D14	M3.8	Sh10	9.81	C	—
I03392+5632	03 39 15.325	+56 32 05.86	189	-55	14.3	2.0	D14	m6.0	L11	9.99	M,W	Y
I03430+4554	03 43 02.068	+45 54 18.15	-210	-27	40.7	1.8	D14	m5.0	L11	9.67	M	Y
I03473+0841	03 47 20.884	+08 41 47.04	459	-657	79.5	3.5	vA95	M4.5	R95	9.85	S	—
I03526+1701	03 52 41.762	+17 01 04.24	427	-636	101.6	2.1	H06	M4.5	R95	8.93	S	—
I03548+1618	03 54 53.220	+16 18 56.32	133	-15	55.4	16.6	PHOT	m5.0	L11	9.96	S	—
I03565+3157	03 56 33.099	+31 57 24.76	104	-47	56.4	16.9	PHOT	M3.0	R07	9.80	S	—
I03588+1230	03 58 49.103	+12 30 23.47	251	-306	36.1	2.9	D14	m5.0	L11	9.76	S	—
I04081+7423	04 08 11.162	+74 23 01.31	664	-591	74.0	22.2	PHOT	m5.0	L11	9.25	S	—
I04122+6443	04 12 17.008	+64 43 55.62	496	-440	84.7	3.0	H93	M4.0	R95	9.16	S	—
I04123+1615	04 12 21.721	+16 15 03.36	154	-24	44.9	3.2	D14	M1.0	BS08	9.74	C	—
I04129+5236	04 12 58.798	+52 36 41.94	-331	-807	83.9	7.0	vA95	M4.5	R95	8.77	BG,C	—
I04173+0849	04 17 18.521	+08 49 22.06	126	-374	67.4	4.5	D14	M4.5	R95	9.03	S	—
I04191+0944	04 19 08.091	+09 44 48.18	34	135	50.7	15.2	PHOT	m5.0	L11	9.99	S	—

Table 1:: continued.

Lepine ID	α (hh mm ss)	δ (dd mm ss)	PM_α (mas)	PM_δ (mas)	π (mas)	e_π (mas)	Ref ^a	Spt ^b	Ref ^c	J (mag)	Mult ^d	ND ^e
I04207+1514	04 20 47.990	+15 14 09.08	171	-56	29.7	2.2	D14	m5.0	L11	9.49	M	Y
I04224+0337	04 22 25.040	+03 37 08.21	139	16	66.5	19.9	PHOT	m5.0	L11	9.86	S	—
I04229+2559	04 22 59.264	+25 59 14.26	37	-237	71.0	21.3	PHOT	M4.0	R04	9.65	S	—
I04234+8055	04 23 29.055	+80 55 10.24	72	-90	71.4	21.4	PHOT	m5.0	L11	9.41	S	—
I04238+1455	04 23 50.352	+14 55 17.37	128	-25	68.7	20.6	PHOT	M3.5	P91	9.29	S	—
I04247-0647	04 24 42.621	-06 47 31.34	154	20	59.6	17.9	PHOT	M4.5	Sh10	9.57	C	—
I04278+1146	04 27 53.524	+11 46 54.83	312	-488	39.8	1.9	D14	M4.0	R95	9.70	S	—
I04290+1840	04 29 01.014	+18 40 25.39	114	-38	64.7	19.4	PHOT	m5.0	L11	9.57	S	—
I04293+1413	04 29 18.479	+14 13 59.50	261	170	79.0	13.0	G91	M4.0	R95	9.35	S	—
I04304+3950	04 30 25.300	+39 50 59.42	269	-568	95.9	2.8	vA95	M4.5	R95	9.11	S	—
I04308-0849S	04 30 52.033	-08 49 19.51	9	-154	64.4	19.3	PHOT	M4.0	R07	9.85	W	—
I04335+2044	04 33 33.970	+20 44 45.77	470	-339	73.4	2.3	D14	M4.0	R95	9.77	S	—
I04360+1853	04 36 04.173	+18 53 18.94	69	-17	64.3	19.3	PHOT	M3.5	U	9.77	S	—
I04382+2813	04 38 12.592	+28 13 00.00	382	-88	82.5	3.1	D14	M4.6	Sh09	8.17	M	N
I04388+2147	04 38 53.542	+21 47 54.64	169	-206	73.9	22.2	PHOT	M3.5	R04	9.55	M,W	Y
I04393+3331	04 39 23.203	+33 31 49.43	16	-40	55.7	16.7	PHOT	M2.5	U	9.92	M	Y
I04398+2509	04 39 48.975	+25 09 26.18	-99	-44	58.1	17.4	PHOT	M3.0	R07	9.64	S	—
I04413+3242	04 41 23.884	+32 42 22.78	256	-149	25.1	1.5	D14	m5.0	L11	9.46	M	Y
I04425+2027	04 42 30.299	+20 27 11.50	76	-18	76.8	23.0	PHOT	m5.0	L11	9.40	C	—
I04472+2038	04 47 12.257	+20 38 10.82	81	-95	110.0	33.0	PHOT	M4.5	R07	9.38	S	—
I04494+4828	04 49 29.473	+48 28 45.90	176	-192	47.1	1.9	D14	M4.0	Sh09	9.06	M	Y
I04499+7109	04 49 55.704	+71 09 47.00	186	-35	41.2	2.0	D14	m5.0	L11	9.63	S	—
I04508+2207	04 50 50.931	+22 07 21.51	632	-426	71.1	5.7	vA95	M5.0	R95	9.90	S	—
I04544+6504	04 54 29.826	+65 04 41.03	55	-113	71.7	21.5	PHOT	m5.0	L11	9.67	S	—
I04559+0440W	04 55 54.456	+04 40 16.44	136	-185	29.0	4.0	G91	m7.0	L11	8.50	S	—
I04560+4313	04 56 03.540	+43 13 55.64	393	-161	70.8	2.4	D14	m5.0	L11	9.30	S	—
I05019-0656	05 01 57.469	-06 56 45.92	-560	-531	187.9	1.3	H06	M4.0	R95	7.62	S	—
I05019+0108	05 01 56.657	+01 08 42.92	23	-92	96.3	28.9	PHOT	M5.0	Sch12	8.53	S	—
I05030+2122	05 03 05.651	+21 22 35.91	104	-131	36.5	8.4	vA95	m4.5	L08	9.75	M	N
I05050+4414	05 05 05.920	+44 14 03.76	98	-18	65.8	19.7	PHOT	m5.0	L11	9.83	S	—
I05062+0439	05 06 12.929	+04 39 27.23	27	-60	89.8	26.9	PHOT	M3.0	A00	8.91	S	—
I05083+7538	05 08 18.461	+75 38 15.37	197	-123	62.3	0.7	G09	M4.5	R03	9.39	M	Y
I05109+1837	05 10 57.438	+18 37 34.55	-237	-647	57.5	1.0	D14	M3.5	R95	9.94	S	—
I05187+4629	05 18 44.555	+46 29 59.64	51	-101	61.2	18.4	PHOT	m5.0	L11	9.96	S	—
I05195+6454	05 19 31.187	+64 54 33.79	6	147	89.3	26.8	PHOT	m5.0	L11	8.95	S	—
I05404+2448	05 40 25.723	+24 48 08.25	104	-370	96.3	2.5	vA95	M5.5	R04	8.98	M	Y
I05424+5038	05 42 25.045	+50 38 41.42	210	-14	37.4	2.0	D14	m5.0	L11	9.91	S	—
I05455-1158	05 45 31.987	-11 58 03.43	57	66	64.9	19.5	PHOT	m5.0	L11	9.59	S	—
I05456+1107	05 45 41.591	+11 07 48.50	96	-96	72.9	21.9	PHOT	m6.0	L11	9.90	S	—
I05484+0745	05 48 24.078	+07 45 38.79	70	-266	45.0	8.0	G91	M4.0	R95	9.78	BG	—
I05566-1018	05 56 40.662	-10 18 37.74	-23	124	84.5	25.3	PHOT	M3.5	R07	9.07	S	—
I05588+2121	05 58 53.322	+21 21 01.47	177	-425	56.0	3.5	D14	M4.5	R04	9.97	M	Y
I05599+5834	05 59 55.693	+58 34 15.32	7	-254	76.0	9.0	G91	M4.2	Sh09	9.03	S	—
I06011+5935	06 01 11.063	+59 35 49.65	-15	-1159	126.0	3.3	K10	M3.5	R95	7.47	S	—
I06024+4951	06 02 29.182	+49 51 56.22	56	-855	107.7	2.6	vA95	M5.0	R95	9.35	S	—
I06034+4748	06 03 29.572	+47 48 14.94	-60	-564	43.2	1.1	D14	M4.0	R95	9.69	S	—
I06054+6049	06 05 29.400	+60 49 22.42	294	-787	71.3	2.2	D14	M4.9	Sh09	9.10	S	—
I06075+4712	06 07 31.859	+47 12 26.38	27	-189	45.2	2.6	D14	M3.5	R07	9.72	S	—
I06102+2234	06 10 17.765	+22 34 19.62	32	-145	43.9	3.7	D14	m5.0	L08	9.88	BG	—
I06145+0230	06 14 34.911	+02 30 27.33	-153	-469	37.8	3.3	vA95	M3.0	S05	9.30	S	—
I06171+0507	06 17 10.646	+05 07 02.43	-201	166	50.0	9.6	vA95	M3.5	R95	9.09	M,W	N
I06185+2503	06 18 34.805	+25 03 05.79	4	-317	37.9	1.0	D14	M4.0	R04	9.95	S	—
I06236-0938	06 23 38.471	-09 38 51.71	-58	12	57.6	17.3	PHOT	M3.5	R04	9.82	M	Y
I06246+2325	06 24 41.292	+23 25 58.98	545	-503	119.4	2.3	vA95	M4.5	R95	8.66	S	—
I06318+4129	06 31 50.735	+41 29 45.51	-14	-204	35.9	7.3	D14	M5.0	R95	9.68	S	—
I06323-0943	06 32 20.290	-09 43 29.10	-7	-49	71.0	21.3	PHOT	m6.0	L11	9.85	S	—
I06325+6406	06 32 30.646	+64 06 20.24	260	-487	46.8	1.9	D14	m5.0	L11	9.81	S	—
I06354-0403	06 35 29.863	-04 03 18.46	-90	74	85.5	25.6	PHOT	m5.0	L11	9.27	M	Y
I06361+1137	06 36 06.389	+11 37 03.06	-214	-861	54.7	2.4	vA95	M4.5	J09	9.79	S	—
I06435+1641	06 43 34.757	+16 41 35.01	-209	34	45.3	2.5	D14	M4.5	R04	9.78	S	—
I06490+3706	06 49 05.451	+37 06 50.60	204	-1580	65.0	3.9	K10	M4.0	R95	9.56	O	—
I06524+1817	06 52 24.315	+18 27 17.94	128	130	53.0	10.0	G91	M3.5	R04	9.05	S	—
I06565+4401	06 56 30.956	+44 01 56.00	192	-677	46.8	3.5	D14	m5.0	L11	9.92	S	—
I06579+6219	06 57 57.081	+62 19 19.25	326	-510	87.4	2.3	vA95	M5.2	Sh09	8.59	M	N
I07033+3441	07 03 23.163	+34 41 51.26	-65	148	73.2	1.8	D14	M4.0	R95	8.77	S	—
I07039+5242	07 03 55.734	+52 42 06.62	679	-914	107.5	1.8	K10	M5.0	R95	8.54	M	N
I07076+4841	07 07 37.758	+48 41 13.53	-28	-298	92.4	3.5	D14	M3.5	R95	9.11	S	—
I07100+3831	07 10 01.851	+38 31 46.53	-440	-948	158.9	3.3	vL07	M4.5	R04	6.73	S	—
I07105-0842	07 10 31.465	-08 42 48.43	-81	98	78.2	23.4	PHOT	m5.0	L11	9.05	S	—
I07111+4329	07 11 11.440	+43 29 58.05	352	-570	77.8	3.0	L09	M6.5	R03	9.98	M,BG	N
I07163+3309	07 16 18.021	+33 09 10.37	-105	-432	66.9	4.1	vA95	M4.0	R95	9.76	S	—

Table 1:: continued.

Lepine ID	α (hh mm ss)	δ (dd mm ss)	PM_α (mas)	PM_δ (mas)	π (mas)	e_π (mas)	Ref ^a	Spt ^b	Ref ^c	J (mag)	Mult ^d	ND ^e
I07172-0501	07 17 17.060	-05 01 03.14	425	-405	102.7	30.8	PHOT	M4.0	R06	8.87	S	—
I07307+4811	07 30 42.777	+48 11 58.66	-226	-1259	80.5	3.0	K10	M4.0	R95	9.14	C,W	—
I07310+4600	07 31 01.291	+46 00 26.55	-13	-93	52.0	15.6	PHOT	M4.0	R06	9.95	S	—
I07320+1719W	07 32 02.131	+17 19 12.07	-234	-204	30.6	3.7	vL07	M3.0	U	9.74	O	—
I07364+0704	07 36 25.135	+07 04 43.13	230	-304	116.6	1.0	H06	M5.0	R95	8.18	M	N
I07365-0039	07 36 30.275	-00 39 35.31	2	-112	68.4	20.5	PHOT	m5.0	L11	9.42	S	—
I07384+2400	07 38 29.500	+24 00 08.66	-179	-100	52.9	2.4	Sh12	M2.7	Sh09	8.93	S	—
I07429-1043	07 42 55.653	-10 43 45.19	-43	-142	63.3	19.0	PHOT	m5.0	L11	9.52	S	—
I07467+5726	07 46 42.028	+57 26 53.19	-44	-230	48.8	1.9	D14	m5.0	L11	9.70	S	—
I07470+7603	07 47 05.863	+76 03 19.24	136	-391	51.2	2.5	D14	M4.0	R04	9.98	S	—
I07518+0532	07 51 51.385	+05 32 57.27	440	-409	62.7	3.1	vA95	M4.5	J09	9.97	S	—
I07519-0000	07 51 54.657	-00 00 11.76	266	-733	114.0	3.3	vA95	M4.5	R04	8.50	S	—
I07558+8323	07 55 53.950	+83 23 04.94	-291	-598	80.3	3.0	vA95	M4.5	GM12	8.74	S	—
I08069+4217	08 06 55.303	+42 17 33.12	-216	-270	52.2	1.2	D14	M4.5	R04	9.72	S	—
I08119+0846	08 11 57.563	+08 46 22.95	1099	-5123	146.3	3.1	vA95	M4.5	R95	8.42	S	—
I08286+6602	08 28 41.223	+66 02 24.03	32	92	73.9	22.2	PHOT	m5.0	L11	9.20	M	Y
I08298+2646	08 29 49.350	+26 46 33.73	-1110	-607	275.8	3.0	vA95	M6.5	MB03	8.23	S	—
I08316+1923	08 31 37.565	+19 23 39.42	-221	-114	90.4	8.2	vL07	M4.0	R95	8.62	M,M,C	N
I08353+1408	08 35 19.907	+14 08 33.21	-151	-77	42.0	1.4	D14	M4.5	R07	9.16	S	—
I08375+0333	08 37 30.220	+03 33 45.84	64	-165	55.4	1.9	D14	m5.0	L11	9.85	S	—
I08413+5929	08 41 20.145	+59 29 50.46	-255	-1277	101.7	3.6	K10	M5.5	R95	9.61	S	—
I08443-1024	08 44 22.364	-10 24 11.12	301	-524	45.0	8.0	G91	M3.5	R95	9.80	S	—
I08563+1239	08 56 19.559	+12 39 49.56	-39	-239	88.0	26.4	PHOT	M4.5	S05	9.59	M	Y
I08582+1945N	08 58 15.125	+19 45 47.02	-858	-46	191.2	2.5	vA95	M5.5	R95	7.79	M	N
I08589+0828	08 58 56.349	+08 28 25.81	379	-338	147.7	2.0	H06	M3.5	R95	6.51	C	—
I08599+7257	08 59 56.199	+72 57 36.44	974	-28	72.6	3.4	vA95	M4.0	R95	9.73	S	—
I09005+4635	09 00 32.468	+46 35 11.42	-471	-519	96.9	2.7	vA95	M4.5	R95	8.60	S	—
I09023+1746	09 02 23.060	+17 46 32.55	-120	-36	58.2	17.5	PHOT	M3.5	R07	9.65	S	—
I09156-1035	09 15 36.405	-10 35 47.18	-381	-174	138.8	41.6	PHOT	M5.5	GM12	8.60	M	N
I09161+0153	09 16 10.188	+01 53 08.85	54	-97	92.3	27.7	PHOT	M4.0	A09	8.77	S	—
I09218+4330	09 21 49.072	+43 30 28.21	-289	-110	46.4	1.8	D14	M4.0	R95	9.43	M	N
I09256+6329	09 25 40.261	+63 29 19.35	-307	-259	53.1	2.5	D14	m5.0	L11	9.82	M	Y
I09410+2201	09 41 02.058	+22 01 28.21	462	-478	79.0	3.8	vA95	M4.5	R95	9.63	S	—
I09449-1220	09 44 54.181	-12 20 54.37	-357	32	132.2	39.7	PHOT	M5.0	R06	8.50	S	—
I09461-0425	09 46 09.287	-04 25 42.98	-554	168	61.0	10.0	G91	M4.0	R95	9.69	M	Y
I09539+2056	09 53 55.184	+20 56 46.81	-332	425	108.4	2.3	H06	M4.5	R95	9.21	S	—
I09564+2239	09 56 26.960	+22 39 01.21	-450	-267	62.0	10.0	G91	M4.0	R95	9.62	S	—
I09589+0557	09 58 56.503	+05 57 59.85	-178	-63	68.2	2.4	D14	m4.5	L08	9.94	S	—
I10416+3736	10 41 37.855	+37 36 39.34	-1450	-362	96.7	2.3	vA95	M4.5	R95	8.49	S	—
I10497+3532	10 49 45.549	+35 32 50.73	-648	-1014	106.5	7.3	K10	M4.5	R95	8.54	C	—
I11509+4822	11 50 57.730	+48 22 38.60	-1534	-953	115.0	5.1	K10	M4.5	R95	8.49	S	—
I11529+2428	11 52 57.898	+24 28 45.47	-302	83	54.0	8.0	G91	M4.5	R95	9.94	S	—
I11582+4234	11 58 17.615	+42 34 28.96	133	-377	56.0	10.0	G91	M4.0	R95	9.59	S	—
I12130+2146	12 13 02.911	+21 46 38.91	43	-142	134.5	40.4	PHOT	m8.0	L11	9.70	M	Y
I12189+1107	12 18 59.407	+11 07 33.83	-1253	209	152.9	3.0	vA95	M5.0	R95	8.52	S	—
I12237+2215	12 23 43.469	+22 15 17.08	-51	-93	127.9	38.4	PHOT	m8.0	L11	9.89	S	—
I12294+2259	12 29 27.125	+22 59 46.74	-159	-21	41.2	2.5	D14	M4.0	Sh09	9.82	S	—
I13143+1320	13 14 20.361	+13 20 00.73	-236	-177	61.0	2.8	L09	M7.0	L09	9.75	C	—
I14170+3142	14 17 02.868	+31 42 47.09	-581	-137	62.2	13.1	vA95	M4.0	R95	8.44	M	N
I14171+0851	14 17 07.317	+08 51 36.34	-126	32	95.1	28.5	PHOT	m5.0	L11	9.11	S	—
I14251+5149	14 25 11.591	+51 49 53.31	-243	-404	68.8	0.1	vL07	m6.0	L11	7.88	S	—
I15100+1921	15 10 04.812	+19 21 27.53	9	-449	58.9	2.7	D14	M4.0	R95	9.06	S	—
I15126+4543	15 12 38.181	+45 43 46.74	-380	356	55.7	13.4	vA95	M4.0	R95	8.98	M	N
I15197+0439	15 19 45.846	+04 39 34.45	32	103	63.7	19.1	PHOT	m5.0	L11	9.55	S	—
I15238+1727	15 23 51.138	+17 27 57.36	-383	-1255	85.1	2.9	vA95	M4.5	R95	9.10	S	—
I15297+4252	15 29 43.982	+42 52 48.90	435	-613	51.1	4.4	vA95	M4.5	R95	9.59	M	Y
I15319+2851	15 31 54.170	+28 51 09.66	-540	36	43.7	2.2	D14	M4.5	R95	9.67	S	—
I15474+4507	15 47 27.422	+45 07 51.51	-247	195	75.2	22.6	PHOT	M4.0	R03	9.08	C	—
I16280+1533	16 28 02.047	+15 33 57.10	-9	-303	41.0	8.0	G91	M2.5	R95	9.38	M	Y
I16555-0823	16 55 35.292	-08 23 40.11	-796	-855	155.4	1.3	C05	M7.0	R95	9.78	W	—
I17033+5124	17 03 23.870	+51 24 22.86	128	613	105.4	2.5	vA95	M5.0	J14	8.77	S	—
I17076+0722	17 07 40.847	+07 22 06.73	-490	-379	78.0	5.3	vA95	M5.0	R95	9.28	M	N
I17176+5224	17 17 38.577	+52 24 22.43	13	-182	57.9	17.4	PHOT	M4.0	S05	9.77	S	—
I17219+2125	17 21 54.624	+21 25 47.44	-164	250	74.6	2.5	D14	M4.0	R95	9.34	S	—
I17281-0143	17 28 11.060	-01 43 57.03	98	-154	56.1	16.8	PHOT	m5.0	L11	9.89	S	—
I17426+7537	17 42 41.558	+75 37 18.85	515	204	72.6	2.5	D14	m5.0	L11	9.68	S	—
I18022+6415	18 02 16.626	+64 15 44.33	207	-384	117.8	3.7	D14	M6.1	Sh09	8.54	S	—
I18054+0132	18 05 29.121	+01 32 35.96	-266	-32	54.5	2.1	D14	m5.0	L11	9.11	S	—
I18068+1720	18 06 48.560	+17 20 47.22	22	174	79.4	2.0	D14	M4.0	R04	9.49	S	—
I18180+3846W	18 18 03.406	+38 46 34.31	-355	-1035	88.4	3.6	vA95	M4.0	R95	9.20	O	—
I18252+1839	18 25 17.981	+18 39 09.12	-115	-42	73.7	22.1	PHOT	m5.0	L11	9.57	S	—

Table 1:: continued.

Lepine ID	α (hh mm ss)	δ (dd mm ss)	PM_α (mas)	PM_δ (mas)	π (mas)	e_π (mas)	Ref ^a	Spt ^b	Ref ^c	J (mag)	Mult ^d	ND ^e
I18354+4545	18 35 27.290	+45 45 40.91	461	366	66.9	2.0	vA95	M3.5	R95	8.89	S	—
I18411+2447S	18 41 09.770	+24 47 14.34	497	88	120.9	7.2	vA95	M4.5	R95	7.53	M	—
I18427+1354	18 42 44.993	+13 54 17.05	-25	354	93.3	11.5	vA95	M4.0	R95	8.36	BG	—
I18453+1851	18 45 22.939	+18 51 58.46	-140	-261	77.8	0.9	D14	m5.0	L11	9.27	S	—
I18491-0315	18 49 06.409	-03 15 17.51	266	-16	86.8	26.0	PHOT	m6.0	L11	9.61	S	—
I19098+1740	19 09 50.867	+17 40 06.40	-638	-417	93.6	2.8	vA95	M4.5	R95	8.82	O	—
I19164+8413	19 16 24.844	+84 13 41.06	-39	139	69.7	20.9	PHOT	m6.0	L11	9.98	S	—
I19260+2426	19 26 01.619	+24 26 17.17	174	100	52.8	1.5	L09	M4.5	R04	9.62	S	—
I19312+3607	19 31 12.561	+36 07 29.93	-120	-99	65.9	2.9	D14	M5.0	Sh10	9.61	W,C	—
I19327-0652	19 32 46.333	-06 52 18.07	-53	-298	50.3	15.1	PHOT	m5.0	L11	9.94	S	—
I19393+1448	19 39 22.090	+14 48 16.02	-32	-46	58.7	17.6	PHOT	m5.0	L11	9.94	S	—
I19452+4043	19 45 12.510	+40 43 18.38	192	24	28.2	3.2	D14	m5.0	L11	8.96	O	—
I19500+3235	19 50 02.454	+32 35 00.48	231	74	58.8	3.4	vA95	M2.5	R95	8.65	M	N
I20021+1300	20 02 10.554	+13 00 31.53	52	-33	68.4	20.5	PHOT	m5.0	L11	9.73	M	Y
I20065+1559	20 06 31.055	+15 59 17.07	188	266	41.6	2.4	D14	m5.0	L11	9.74	S	—
I20082+3318	20 08 17.908	+33 18 12.87	339	381	46.2	5.4	vA95	M4.5	R04	9.96	S	—
I20260+5834	20 26 05.288	+58 34 22.53	268	552	107.5	3.6	vA95	M5.0	R95	9.03	S	—
I20283+6143	20 28 19.197	+61 43 47.89	-289	-7	76.2	22.9	PHOT	m5.0	L11	9.32	S	—
I20298+0941	20 29 48.325	+09 41 20.19	665	138	113.8	1.9	vA95	M4.5	R95	8.23	M	N
I20300+0023	20 30 01.919	+00 23 55.33	115	12	67.4	20.2	PHOT	m5.0	L11	9.91	M	Y
I20314+3833	20 31 25.642	+38 33 44.34	202	723	67.1	2.8	vA95	M4.0	R95	9.19	M	Y
I20332+2823	20 33 15.806	+28 23 44.45	-241	-287	45.7	1.4	D14	m5.0	L11	9.96	S	—
I20337+2322	20 33 42.751	+23 22 13.80	310	86	45.0	9.0	G91	M3.0	R95	9.11	M	Y
I20349+5917	20 34 55.298	+59 17 26.86	-243	-43	46.4	1.7	D14	M3.5	R95	9.32	S	—
I20367+3850	20 36 46.033	+38 50 32.76	173	-147	49.0	9.0	G91	M3.5	R95	9.27	S	—
I20405+1529	20 40 33.867	+15 29 58.85	1323	667	102.0	2.2	vA95	M4.5	R95	8.64	S	—
I20433+5520	20 43 19.263	+55 20 53.03	872	1720	63.0	5.5	vA95	M5.0	R95	9.56	C	—
I20488+1943	20 48 52.449	+19 43 04.86	-162	-191	29.8	1.8	vA95	M4.0	R95	9.24	M	Y
I20535+1037	20 53 33.061	+10 37 02.27	-496	-441	71.9	2.8	vA95	M4.0	R95	9.35	S	—
I20593+5303	20 59 20.361	+53 03 04.93	168	28	19.5	3.4	D14	m4.5	L08	9.91	M	Y
I21000+4004E	21 00 05.405	+40 04 13.36	614	-247	65.4	1.8	vL07	M3.0	R04	6.67	M,C	N
I21013+3314	21 01 20.632	+33 14 27.97	302	-132	59.0	8.0	G91	M3.5	R95	8.94	M	Y
I21014+2043	21 01 24.836	+20 43 38.10	-389	-393	44.1	1.2	D14	M3.5	R95	9.94	M	Y
I21027+3454	21 02 46.091	+34 54 35.61	233	-263	33.7	1.9	D14	M4.5	R04	9.85	S	—
I21057+5015W	21 05 42.437	+50 15 57.70	103	38	55.5	16.6	PHOT	m5.0	L11	9.97	S	—
I21109+4657S	21 10 58.784	+46 57 32.14	-220	-314	92.2	27.7	PHOT	M2.5	R04	9.88	BG	—
I21127-0719	21 12 45.586	-07 19 55.82	102	-37	70.6	21.2	PHOT	m6.0	L11	9.90	S	—
I21160+2951E	21 16 05.801	+29 51 51.21	204	39	65.0	9.0	G91	M3.3	Sh09	8.45	W,C	—
I21173+2053N	21 17 22.639	+20 53 58.55	308	303	45.6	12.6	vA95	M3.0	R95	8.91	M	N
I21376+0137	21 37 40.188	+01 37 13.76	83	-54	95.1	28.5	PHOT	M5.0	Sch12	8.80	M	Y
I21466+6648S	21 46 40.232	+66 48 10.64	390	211	73.2	3.1	D14	m6.0	L11	8.84	S	—
I21472-0444	21 47 17.461	-04 44 40.62	256	12	91.3	27.4	PHOT	m6.0	L11	9.42	S	—
I21554+5938	21 55 24.360	+59 38 37.15	107	27	90.6	27.2	PHOT	M4.0	M98	9.18	M	Y
I22035+0340	22 03 33.384	+03 40 23.64	7	-106	67.3	20.2	PHOT	m5.0	L11	9.74	M	Y
I22067+0325	22 06 46.362	+03 25 03.90	470	-311	53.0	12.0	G91	M4.0	R95	9.41	S	—
I22088+1144	22 08 50.347	+11 44 13.22	89	-49	58.0	17.4	PHOT	m5.0	L11	9.90	S	—
I22095+1152	22 09 31.677	+11 52 53.54	163	-119	51.9	15.6	PHOT	m5.0	L11	9.90	S	—
I22114+4059	22 11 24.162	+40 59 58.79	-89	68	102.9	30.9	PHOT	m7.0	L11	9.73	S	—
I22154+6613	22 15 26.162	+66 13 27.66	6	210	60.0	12.0	G91	M3.5	R95	8.75	S	—
I22300+4851	22 30 04.182	+48 51 34.66	-77	-66	62.2	18.7	PHOT	m5.0	L11	9.52	M	Y
I22387+2513	22 38 44.311	+25 13 30.51	284	7	62.0	18.6	PHOT	M3.5	R04	9.77	O	—
I22489+1819	22 48 54.595	+18 19 59.00	-22	-122	62.2	18.7	PHOT	m5.0	L11	9.96	S	—
I22509+4959	22 50 55.071	+49 59 13.23	121	-6	70.3	21.1	PHOT	m5.0	L11	9.80	S	—
I23006+0338	23 00 36.123	+03 38 16.96	309	42	61.0	18.3	PHOT	m5.0	L11	9.59	S	—
I23028+4338	23 02 52.493	+43 38 15.69	-156	-16	79.5	1.8	D14	M4.0	R07	9.32	S	—
I23182+7934	23 18 16.912	+79 34 47.51	502	-101	57.3	17.2	PHOT	m5.0	L11	9.71	S	—
I23256+5308	23 25 40.290	+53 08 06.01	984	330	40.4	3.1	vA95	M4.5	R95	9.88	S	—
I23317-0625	23 31 47.637	-06 25 50.41	-28	-151	55.7	16.7	PHOT	M4.5	R07	9.84	S	—
I23318+1956E	23 31 52.537	+19 56 13.89	603	17	161.8	1.7	vL07	M4.5	R95	7.10	W	—
I23351-0223	23 35 10.503	-02 23 21.44	762	-835	138.3	3.5	vA95	M5.5	D98	9.15	S	—
I23419+4410	23 41 55.005	+44 10 38.92	109	-1579	315.7	1.4	G08	M5.0	R95	6.88	S	—
I23425+3914	23 42 33.501	+39 14 23.35	32	-219	87.7	26.3	PHOT	m6.0	L11	9.64	S	—
I23428+3049	23 42 52.734	+30 49 21.83	-332	-290	81.8	2.6	vA95	M4.5	R95	9.64	S	—
I23438+6102	23 43 53.298	+61 02 15.57	-609	-485	54.9	1.7	D14	m5.0	L11	9.39	S	—
I23505-0933	23 50 31.589	-09 33 32.06	634	-418	62.4	1.7	R10	M4.0	R95	8.94	S	—
I23509+3829	23 50 54.031	+38 29 33.39	-90	-195	47.9	2.5	D14	M4.0	R95	9.80	S	—

Table 1:: continued.

Lepine ID	α (hh mm ss)	δ (dd mm ss)	PM_α (mas)	PM_δ (mas)	π (mas)	e_π (mas)	Ref ^a	SpT ^b	Ref ^c	J (mag)	Mult ^d	ND ^e

^aReferences for parallax. PHOT means photometric parallax from Lépine & Gaidos (2011), all other are trigonometric parallaxes.

C05: Costa et al. (2005), D14: Dittmann et al. (2014), G91: Gliese & Jahreiss (1991), G08: Gatewood (2008), G09: Gatewood & Coban (2009), H93: Harrington et al. (1993), H06: Henry et al. (2006), K10: Khrustkaya et al. (2010), L09: Lépine et al. (2009), M92: Monet et al. (1992), R10: Riedel et al. (2010), Sh12: Shkolnik et al. (2012), va95: van Altena et al. (1995), vL07: van Leeuwen (2007).

^bSpectral type; lower case notation implies a color-based SpT estimation which may be biased, see text.

^cReferences for spectral type. A00: Alcalá et al. (2000), A09: Agüeros et al. (2009), BS08: Bender & Simon (2008), D98: Delfosse et al. (1998), F09: Faherty et al. (2009), J14: Jao et al. (2014), J09: Jenkins et al. (2009), L09: Lépine et al. (2009), M13: Mann et al. (2013).

M03: Mohanty et al. (2003), M98: Motch et al. (1998), P91: Prosser et al. (1991), R95: Reid et al. (1995), R03: Reid et al. (2003),

R04: Reid et al. (2004), R07: Reid et al. (2007), S05: Scholz et al. (2005), Sch12: Schlieder et al. (2012a), Sh09: Shkolnik et al. (2009).

U: Unknown, spectral type listed in SIMBAD but it was not possible to locate the source.

^dMultiplicity flag. S: Single, as far as is known. M: Multiple within the AstralLux sensitivity range. C: A known companion exists in the literature but is too close in for AstralLux. W: A known companion exists outside of the AstralLux completeness range. O: An object is observed in the AstralLux image, but is outside of the completeness range. BG: One or more suspected or confirmed background objects are observed in the images. See individual notes for detailed comments.

^eFlag for whether the companion is a new discovery (Y) or not (N).

Table 2:: Astrometric properties of the binaries and background stars in the survey.

Lepine ID	Other ID	Pair	ρ ($''$)	θ (deg)	Epoch (yr)	Ref ^a	CPM ^b	OM ^c
I00066-0705	—	AB	0.230 \pm 0.006	6.5 \pm 0.5	2008.63	J12	Y	Y
I00066-0705	—	AB	0.322 \pm 0.004	1.9 \pm 0.3	2012.65	TP		
I00066-0705	—	AB	0.337 \pm 0.003	1.4 \pm 0.3	2012.90	TP		
I00077+6022	G 217-32	AB	0.612 \pm 0.006	82.5 \pm 0.3	2011.85	TP	Y	Y
I00077+6022	G 217-32	AB	0.661 \pm 0.007	86.9 \pm 0.3	2012.65	TP		
I00077+6022	G 217-32	AB	0.674 \pm 0.007	87.9 \pm 0.3	2012.89	TP		
I00088+2050	GJ 3010	AB	0.111 \pm 0.005	169.9 \pm 0.5	2001.60	B04	Y	Y
I00088+2050	GJ 3010	AB	0.133 \pm 0.005	271.9 \pm 1.7	2012.02	TP		
I00132+6919N	GJ 11 B	AB	0.700 \pm 0.100	319.0 \pm 5.0	1935.50	WDS	Y	Y
I00132+6919N	GJ 11 B	AB	0.859 \pm 0.009	89.2 \pm 0.3	2012.02	TP		
I00395+1454N	G 32-37 B	AB	0.151 \pm 0.002	223.9 \pm 1.7	2012.90	TP	I	—
I00489+4435	GJ 3058	AB	1.050 \pm 0.011	254.1 \pm 0.3	2008.03	J12	Y	Y
I00489+4435	GJ 3058	AB	1.027 \pm 0.010	255.5 \pm 0.3	2012.02	TP		
I01032+7113	LHS 1182	AB	0.147 \pm 0.003	34.2 \pm 0.7	2012.01	TP	I	—
I01114+1526	GJ 3076	AB	0.309 \pm 0.003	186.1 \pm 0.3	2006.86	J12	Y	Y
I01114+1526	GJ 3076	AB	0.303 \pm 0.005	231.6 \pm 0.5	2011.85	TP		
I01114+1526	GJ 3076	AB	0.308 \pm 0.004	238.4 \pm 0.3	2012.65	TP		
I01114+1526	GJ 3076	AB	0.327 \pm 0.015	241.1 \pm 0.8	2012.89	TP		
I01431+2101	—	AB	0.355 \pm 0.004	325.8 \pm 0.3	2012.02	TP	I	—
I02019+7332	GJ 3125	AB	0.438 \pm 0.004	266.3 \pm 0.3	2011.86	TP	Y	Y
I02019+7332	GJ 3125	AB	0.436 \pm 0.004	260.2 \pm 0.3	2012.65	TP		
I02019+7332	GJ 3125	AB	0.437 \pm 0.004	258.8 \pm 0.6	2012.89	TP		
I02133+3648	—	AB	0.181 \pm 0.002	56.5 \pm 2.2	2007.61	J12	Y	Y
I02133+3648	—	AB	0.226 \pm 0.008	81.7 \pm 0.6	2012.66	TP		
I02133+3648	—	AB	0.217 \pm 0.004	76.1 \pm 0.5	2012.90	TP		
I02562+2359	—	AB	0.107 \pm 0.003	98.4 \pm 2.3	2012.02	TP	I	—
I03194+6156	G 246-33	AB	0.380 \pm 0.004	242.8 \pm 0.3	2012.02	TP	Y	Y
I03194+6156	G 246-33	AB	0.387 \pm 0.004	240.9 \pm 0.3	2012.66	TP		
I03194+6156	G 246-33	AB	0.386 \pm 0.004	239.8 \pm 0.3	2012.90	TP		
I03257+0551	GJ 3224	AB	0.275 \pm 0.006	69.0 \pm 0.3	2012.67	TP	I	—
I03257+0551	GJ 3224	AC	2.011 \pm 0.020	209.2 \pm 0.3	2012.01	TP	Y	U
I03257+0551	GJ 3224	AC	2.086 \pm 0.128	210.6 \pm 2.8	2012.67	TP		
I03263+1709	—	AB	0.899 \pm 0.009	221.3 \pm 0.3	2012.01	TP	Y	Y
I03263+1709	—	AB	0.945 \pm 0.010	222.9 \pm 0.3	2012.90	TP		
I03309+7041S	LHS 1553	AB	0.354 \pm 0.004	315.2 \pm 0.3	2012.02	TP	I	—
I03325+2843	—	AB	0.540 \pm 0.005	106.4 \pm 0.3	2006.86	J12	Y	Y
I03325+2843	—	AB	0.482 \pm 0.005	105.5 \pm 0.3	2012.02	TP		
I03325+2843	—	BC	0.135 \pm 0.016	285.5 \pm 2.0	2006.86	J12		
I03325+2843	—	BC	0.098 \pm 0.003	282.4 \pm 3.9	2012.02	TP		
I03392+5632	G 175-2	AB	0.340 \pm 0.003	211.6 \pm 0.3	2012.02	TP	Y	Y
I03392+5632	G 175-2	AB	0.347 \pm 0.004	212.3 \pm 0.3	2012.65	TP		
I03392+5632	G 175-2	AB	0.354 \pm 0.004	214.5 \pm 0.3	2012.89	TP		
I03430+4554	NLTT 11633	AB	0.884 \pm 0.009	310.8 \pm 0.3	2012.02	TP	Y	N
I03430+4554	NLTT 11633	AB	0.888 \pm 0.009	309.9 \pm 0.3	2012.90	TP		
I04129+5236	LHS 1642	AB	2.634 \pm 0.026	332.1 \pm 0.3	2012.02	TP	—	BG?
I04207+1514	LP 475-7	AB	0.220 \pm 0.003	91.2 \pm 0.4	2012.90	TP	I	—
I04382+2813	GJ 3304	AB	0.783 \pm 0.002	300.6 \pm 0.1	2005.79	D07	Y	Y
I04382+2813	GJ 3304	AB	1.105 \pm 0.011	303.3 \pm 0.3	2012.02	TP		
I04388+2147	G 8-48	AB	1.232 \pm 0.012	125.9 \pm 0.3	2012.02	TP	I	—

Table 2:: continued.

Lepine ID	Other ID	Pair	ρ ($''$)	θ (deg)	Epoch	Ref ^a	CPM ^b	OM ^c
I04393+3331	—	AB	0.126 \pm 0.003	50.6 \pm 1.2	2012.02	TP	—	—
I04413+3242	—	AB	1.479 \pm 0.015	0.9 \pm 0.3	2012.02	TP	I	—
I04494+4828	G 81-34	AB	0.635 \pm 0.006	239.0 \pm 0.3	2012.02	TP	I	—
I05030+2122	LP 359-186	AB	0.310 \pm 0.010	171.6 \pm 1.4 ^d	2005.90	L08	Y	N
I05030+2122	LP 359-186	AB	0.339 \pm 0.009	166.7 \pm 0.3	2011.86	TP	—	—
I05030+2122	LP 359-186	AB	0.302 \pm 0.011	167.7 \pm 1.1	2012.89	TP	—	—
I05083+7538	G 248-32	AB	0.191 \pm 0.002	211.7 \pm 0.7	2012.02	TP	I	—
I05404+2448	GJ 1083	AB	0.557 \pm 0.006	323.7 \pm 0.3	2011.86	TP	Y	Y
I05404+2448	GJ 1083	AB	0.472 \pm 0.008	337.0 \pm 0.3	2012.89	TP	—	—
I05484+0745	G 106-2	AB	1.623 \pm 0.016	17.3 \pm 0.3	2011.86	TP	—	BG?
I05588+2121	LHS 6097	AB	0.488 \pm 0.005	100.4 \pm 0.3	2011.86	TP	Y	Y
I05588+2121	LHS 6097	AB	0.455 \pm 0.005	99.8 \pm 0.4	2012.90	TP	—	—
I06102+2234	—	AB	1.855 \pm 0.019	327.3 \pm 0.3	2012.02	TP	—	BG?
I06171+0507	NLTT 16333	AB	0.431 \pm 0.004	157.9 \pm 0.7	2006.12	P06	Y	Y
I06171+0507	NLTT 16333	AB	0.618 \pm 0.006	157.7 \pm 0.3	2012.01	TP	—	—
I06236-0938	—	AB	1.832 \pm 0.018	272.6 \pm 0.3	2012.01	TP	—	—
I06354-0403	—	AB	0.155 \pm 0.006	170.6 \pm 1.2	2012.01	TP	—	—
I06579+6219	GJ 3417	AB	1.526 \pm 0.010	230.2 \pm 1.0 ^d	2005.90	L08	Y	Y
I06579+6219	GJ 3417	AB	1.441 \pm 0.014	239.7 \pm 0.3	2012.02	TP	—	—
I07039+5242	LHS 224	AB	0.163 \pm 0.005	344.7 \pm 0.5	2000.30	B04	Y	Y
I07039+5242	LHS 224	AB	0.127 \pm 0.003	185.9 \pm 1.6	2012.02	TP	—	—
I07111+4329	—	AB	0.275 \pm 0.005	208.0 \pm 0.5	2004.02	D10	Y	Y
I07111+4329	—	AB	0.348 \pm 0.004	188.0 \pm 0.4	2011.85	TP	—	—
I07111+4329	—	AC	2.856 \pm 0.029	136.0 \pm 0.3	2011.85	TP	—	BG?
I07364+0704	GJ 3454	AB	0.898 \pm 0.010	61.3 \pm 1.0	2005.90	L08	Y	Y
I07364+0704	GJ 3454	AB	0.674 \pm 0.007	11.4 \pm 0.3	2011.85	TP	—	—
I08286+6602	—	AB	0.294 \pm 0.003	146.4 \pm 0.3	2012.01	TP	I	—
I08316+1923	CU Cnc	AaAb	0.682 \pm 0.005	158.0 \pm 0.5	2000.13	B04	Y	Y
I08316+1923	CU Cnc	AaAb	0.536 \pm 0.012	181.1 \pm 1.3	2011.85	TP	—	—
I08316+1923	CU Cnc	BaBb	0.549 \pm 0.005	219.1 \pm 0.5	2000.13	B04	Y	Y
I08316+1923	CU Cnc	BaBb	0.957 \pm 0.010	190.9 \pm 0.3	2011.85	TP	—	—
I08563+1239	G 41-8	AB	1.824 \pm 0.018	210.3 \pm 0.3	2011.85	TP	I	—
I08582+1945N	LHS 2077	AB	1.391 \pm 0.010	256.6 \pm 1.0	2005.90	L08	Y	Y
I08582+1945N	LHS 2077	AB	1.843 \pm 0.018	211.3 \pm 0.3	2012.02	TP	—	—
I09156-1035	LHS 6167	AB	0.076 \pm 0.001	82.4 \pm 0.3	2003.70	M06	Y	Y
I09156-1035	LHS 6167	AB	0.123 \pm 0.003	175.7 \pm 1.4	2012.01	TP	—	—
I09218+4330	GJ 3554	AB	0.579 \pm 0.010	44.0 \pm 1.1	2005.90	L08	Y	Y
I09218+4330	GJ 3554	AB	0.687 \pm 0.007	128.0 \pm 0.3	2011.86	TP	—	—
I09256+6329	G 235-25	AB	0.126 \pm 0.004	92.7 \pm 1.7	2012.01	TP	I	—
I09461-0425	LHS 2186	AB	1.153 \pm 0.012	358.3 \pm 0.3	2012.01	TP	I	—
I12130+2146	—	AB	0.576 \pm 0.006	255.4 \pm 0.3	2012.43	TP	—	—
I14170+3142	GJ 3839	AB	0.694 \pm 0.010	338.5 \pm 1.0	2005.40	L08	Y	Y
I14170+3142	GJ 3839	AB	0.439 \pm 0.004	218.6 \pm 0.3	2012.43	TP	—	—
I15126+4543	GJ 3898	AB	0.790 \pm 0.050	194.1 \pm 0.3	1997.30	M01	Y	Y
I15126+4543	GJ 3898	AB	0.549 \pm 0.006	216.7 \pm 0.3	2012.43	TP	—	—
I15297+4252	LHS 3075	AB	0.570 \pm 0.006	8.8 \pm 0.3	2012.43	TP	I	—
I16280+1533	G 138-33	AB	0.558 \pm 0.006	35.1 \pm 0.3	2012.43	TP	I	—
I17076+0722	GJ 1210	AB	0.183 \pm 0.005	266.7 \pm 0.5	2008.47	H12	Y	Y
I17076+0722	GJ 1210	AB	0.436 \pm 0.004	236.3 \pm 0.3	2012.43	TP	—	—
I18411+2447S	GJ 1230	AB	9.000 \pm 0.500	12.0 \pm 5.0	1960.50	WDS	Y	Y
I18411+2447S	GJ 1230	AB	4.833 \pm 0.048	5.6 \pm 0.3	2012.43	TP	—	—
I18427+1354	GJ 4071	AB	3.695 \pm 0.037	176.6 \pm 0.3	2012.66	TP	—	BG?
I19500+3235	LHS 3489	AB	0.378 \pm 0.010	274.2 \pm 2.0	2008.43	J13	Y	Y
I19500+3235	LHS 3489	AB	0.238 \pm 0.002	340.0 \pm 0.4	2012.43	TP	—	—
I19500+3235	LHS 3489	AB	0.235 \pm 0.002	340.7 \pm 0.3	2012.43	TP	—	—
I19500+3235	LHS 3489	AB	0.222 \pm 0.002	345.1 \pm 0.7	2012.67	TP	—	—
I20021+1300	—	AB	0.261 \pm 0.004	42.9 \pm 0.5	2012.43	TP	—	—
I20298+0941	HU Del	AB	0.160 \pm 0.002	89.1 \pm 2.3	2012.66	TP	I	—
I20300+0023	—	AB	0.398 \pm 0.004	354.3 \pm 0.3	2012.66	TP	—	—
I20314+3833	LHS 3559	AB	0.118 \pm 0.006	252.4 \pm 1.4	2012.66	TP	I	—
I20337+2322	G 186-29	AB	0.906 \pm 0.009	176.2 \pm 0.3	2012.66	TP	I	—
I20488+1943	G 144-39	AB	0.219 \pm 0.002	133.6 \pm 0.8	2012.67	TP	I	—
I20593+5303	—	AB	0.433 \pm 0.004	23.2 \pm 0.7	2012.01	TP	Y	N
I20593+5303	—	AB	0.445 \pm 0.004	20.9 \pm 0.4	2012.67	TP	—	—
I20593+5303	—	AB	0.444 \pm 0.004	21.4 \pm 0.4	2012.90	TP	—	—
I21000+4004E	GJ 815	AB	0.609 \pm 0.006	29.7 \pm 0.3	2011.86	TP	Y	Y
I21000+4004E	GJ 815	AB	0.668 \pm 0.007	37.1 \pm 0.3	2012.65	TP	—	—
I21000+4004E	GJ 815	AB	0.685 \pm 0.007	39.0 \pm 0.3	2012.90	TP	—	—
I21013+3314	G 187-14	AB	0.142 \pm 0.003	34.0 \pm 0.3	2012.01	TP	I	—
I21014+2043	LHS 3610	AB	0.392 \pm 0.008	41.9 \pm 0.6	2012.67	TP	I	—
I21109+4657S	G 212-27	AB	2.053 \pm 0.021	35.0 \pm 0.3	2011.86	TP	N	BG

Table 2:: continued.

Lepine ID	Other ID	Pair	ρ ($''$)	θ (deg)	Epoch (yr)	Ref ^a	CPM ^b	OM ^c
I21109+4657S	G 212-27	AB	2.332 \pm 0.023	35.8 \pm 0.3	2012.66	TP		
I21109+4657S	G 212-27	AB	2.437 \pm 0.024	35.5 \pm 0.3	2012.89	TP		
I21109+4657S	G 212-27	AC	3.710 \pm 0.037	191.7 \pm 0.3	2011.86	TP		
I21109+4657S	G 212-27	AC	3.478 \pm 0.035	190.0 \pm 0.3	2012.66	TP		
I21109+4657S	G 212-27	AC	3.356 \pm 0.034	189.0 \pm 0.3	2012.89	TP		
I21173+2053N	G 145-31	AB	3.800 \pm 0.500	347.0 \pm 5.0	1960.50	WDS	Y	N
I21173+2053N	G 145-31	AB	4.281 \pm 0.043	341.3 \pm 0.3	2012.66	TP		
I21376+0137	—	AB	0.433 \pm 0.004	341.1 \pm 0.3	2012.67	TP	—	—
I21554+5938	—	AB	0.199 \pm 0.002	102.3 \pm 0.3	2012.02	TP	—	—
I22035+0340	—	AB	0.412 \pm 0.004	351.9 \pm 0.3	2012.66	TP	—	—
I22300+4851	—	AB	2.300 \pm 0.023	252.9 \pm 0.3	2012.02	TP	I	—

^aSource of the astrometry at the given epoch. Only one archival epoch listed per target.

TP: This paper.

WDS: Washington Double Star Catalog, Mason et al. (2001).

M01: McCarthy et al. (2001).

B04: Beuzit et al. (2004); uniform errors assumed.

M06: Montagnier et al. (2006).

P06: Pravdo et al. (2006).

D07: Daemgen et al. (2007).

L08: Law et al. (2008).

D10: Dupuy et al. (2010) orbital analysis; original data point from Montagnier et al. (2006).

H12: Horch et al. (2012).

J12: Janson et al. (2012).

J13: Jódar et al. (2013).

^bFlag for common proper motion (evaluated between the first and last listed epochs), yes (Y), no (N) or inferred (I).^cFlag for orbital motion (between the first and last listed epochs), yes (Y), no (N), unclear (U), or background (BG).^dQuoted angle assumes a phase shift, see individual note for the target.

Table 3:: Photometric and physical properties of the binaries in the survey.

Lepine ID	Other ID	Pair	$\Delta z'$ (mag)	$\Delta i'$ (mag)	τ_{low} (Myr)	τ_{high} (Myr)	Ref ^a	m_A (M_{\odot})	m_B (M_{\odot})	q	a_{est} (AU)	SC ^b
I00066-0705	—	AB	1.15 \pm 0.05	1.43 \pm 0.04	1000	10000	NY	0.35 \pm 0.09	0.21 \pm 0.05	0.61 \pm 0.05	5.6	N
I00077+6022	G 217-32	AB	0.72 \pm 0.12	0.86 \pm 0.16	35	300	Sh12	0.17 \pm 0.07	0.12 \pm 0.06	0.68 \pm 0.06	9.8	Y
I00088+2050	GJ 3010	AB	1.20 \pm 0.07	1.59 \pm 0.10	30	300	VY	0.20 \pm 0.09	0.11 \pm 0.06	0.52 \pm 0.05	2.0	Y
I00132+6919N	GJ 11 B	AB	0.81 \pm 0.01	0.69 \pm 0.02	1000	10000	NY	0.38 \pm 0.10	0.26 \pm 0.06	0.69 \pm 0.02	17.2	Y
I00395+1454N	G 32-37 B	AB	1.12 \pm 0.10	—	300	1000	MY	0.33 \pm 0.03	0.19 \pm 0.01	0.58 \pm 0.01	4.3	N
I00489+4435	GJ 3058	AB	0.28 \pm 0.01	0.35 \pm 0.02	50	150	Sc12	0.22 \pm 0.10	0.18 \pm 0.08	0.84 \pm 0.01	19.0	Y
I01032+7113	LHS 1182	AB	1.47 \pm 0.06	1.62 \pm 0.07	1000	10000	NY	0.21 \pm 0.04	0.13 \pm 0.02	0.59 \pm 0.05	2.7	Y
I01114+1526	GJ 3076	AB	1.71 \pm 0.86	1.46 \pm 0.15	10	20	M13	0.10 \pm 0.03	0.04 \pm 0.01	0.45 \pm 0.06	5.6	Y
I01431+2101	—	AB	1.40 \pm 0.06	1.41 \pm 0.07	300	1000	MY	0.30 \pm 0.06	0.15 \pm 0.03	0.51 \pm 0.01	4.8	Y
I02019+7332	GJ 3125	AB	1.25 \pm 0.23	1.37 \pm 0.29	30	300	VY	0.12 \pm 0.07	0.06 \pm 0.04	0.49 \pm 0.11	5.0	Y
I02133+3648	—	AB	2.16 \pm 0.15	2.42 \pm 0.18	30	300	VY	0.26 \pm 0.06	0.09 \pm 0.03	0.33 \pm 0.04	2.8	Y
I02562+2359	—	AB	1.50 \pm 0.06	1.89 \pm 0.16	1000	10000	NY	0.07 \pm 0.02	0.07 \pm 0.01	0.90 \pm 0.13	0.4	N
I03194+6156	G 246-33	AB	1.02 \pm 0.21	1.19 \pm 0.22	35	300	Sh12	0.29 \pm 0.11	0.17 \pm 0.07	0.58 \pm 0.05	10.8	Y
I03257+0551	GJ 3224	AB	1.23 \pm 1.08	1.63 \pm 1.24	300	1000	MY	0.25 \pm 0.06	0.14 \pm 0.01	0.58 \pm 0.09	6.3	N
I03257+0551	GJ 3224	AC	0.22 \pm 0.00	0.17 \pm 0.01	300	1000	MY	0.48 \pm 0.25	0.45 \pm 0.24	0.94 \pm 0.02	48.1	N
I03263+1709	—	AB	0.95 \pm 0.53	1.02 \pm 0.65	1000	10000	NY	0.24 \pm 0.03	0.16 \pm 0.03	0.69 \pm 0.09	20.6	N
I03309+7041S	LHS 1553	AB	1.46 \pm 0.09	1.63 \pm 0.10	1000	10000	NY	0.31 \pm 0.03	0.17 \pm 0.02	0.54 \pm 0.04	7.9	Y
I03325+2843	—	AB	0.78 \pm 0.28	1.09 \pm 0.08	10	20	Sc12	0.07 \pm 0.01	0.04 \pm 0.01	0.59 \pm 0.05	8.7	Y
I03392+5632	G 175-2	AB	1.53 \pm 0.98	1.61 \pm 0.73	1000	10000	NY	0.60 \pm 0.10	0.38 \pm 0.03	0.63 \pm 0.05	24.7	N
I03430+4554	NLTT 11633	AB	0.77 \pm 0.28	0.89 \pm 0.20	1000	10000	NY	0.28 \pm 0.03	0.20 \pm 0.04	0.73 \pm 0.07	21.8	N
I04207+1514	LP 475-7	AB	1.71 \pm 0.06	1.89 \pm 0.03	1000	10000	NY	0.45 \pm 0.04	0.21 \pm 0.03	0.47 \pm 0.03	7.4	Y
I04382+2813	GJ 3304	AB	0.66 \pm 0.01	0.67 \pm 0.01	60	300	Sh12	0.28 \pm 0.06	0.19 \pm 0.05	0.68 \pm 0.03	13.4	Y
I04388+2147	G 8-48	AB	0.35 \pm 0.01	0.55 \pm 0.02	300	1000	MY	0.12 \pm 0.04	0.10 \pm 0.03	0.90 \pm 0.05	21.9	N
I04393+3331	—	AB	1.21 \pm 0.05	1.36 \pm 0.06	1000	10000	NY	0.32 \pm 0.16	0.20 \pm 0.10	0.63 \pm 0.04	2.6	Y
I04413+3242	—	AB	0.72 \pm 0.01	0.94 \pm 0.01	300	1000	MY	0.54 \pm 0.04	0.40 \pm 0.06	0.74 \pm 0.05	58.9	Y
I04494+4828	G 81-34	AB	0.74 \pm 0.03	0.82 \pm 0.04	30	300	VY	0.27 \pm 0.14	0.18 \pm 0.09	0.66 \pm 0.02	13.5	Y
I05030+2122	LP 359-186	AB	2.37 \pm 0.34	1.98 \pm 0.18	1000	10000	NY	0.38 \pm 0.03	0.16 \pm 0.01	0.43 \pm 0.01	8.3	Y
I05083+7538	G 248-32	AB	0.86 \pm 0.03	1.00 \pm 0.03	1000	10000	NY	0.21 \pm 0.04	0.15 \pm 0.03	0.72 \pm 0.09	3.1	Y
I05404+2448	GJ 1083	AB	1.08 \pm 0.06	0.98 \pm 0.07	1000	10000	NY	0.20 \pm 0.04	0.13 \pm 0.02	0.66 \pm 0.06	4.9	Y
I05588+2121	LHS 6097	AB	1.62 \pm 0.10	2.27 \pm 0.25	1000	10000	NY	0.20 \pm 0.04	0.10 \pm 0.01	0.52 \pm 0.06	8.1	N
I06171+0507	NLTT 16333	AB	2.07 \pm 0.06	2.36 \pm 0.14	1000	10000	NY	0.39 \pm 0.06	0.15 \pm 0.02	0.39 \pm 0.03	11.9	Y
I06236-0938	—	AB	2.39 \pm 0.01	—	1000	10000	NY	0.32 \pm 0.19	0.12 \pm 0.05	0.45 \pm 0.16	33.5	Y
I06354-0403	—	AB	1.96 \pm 0.13	2.28 \pm 0.10	1000	10000	NY	0.31 \pm 0.03	0.14 \pm 0.01	0.43 \pm 0.00	2.0	Y
I06579+6219	GJ 3417	AB	1.36 \pm 0.01	1.60 \pm 0.02	60	300	Sh12	0.30 \pm 0.14	0.15 \pm 0.08	0.49 \pm 0.05	16.5	Y
I07039+5242	LHS 224	AB	0.54 \pm 0.09	0.78 \pm 0.05	1000	10000	NY	0.18 \pm 0.03	0.14 \pm 0.01	0.81 \pm 0.07	1.2	Y
I07111+4329	—	AB	1.60 \pm 0.09	2.03 \pm 0.12	1000	10000	NY	0.15 \pm 0.03	0.09 \pm 0.01	0.60 \pm 0.10	4.5	N

Table 3:: continued.

Lepine ID	Other ID	Pair	$\Delta z'$ (mag)	$\Delta i'$ (mag)	τ_{low} (Myr)	τ_{high} (Myr)	Ref ^a	m_A (M_{Sun})	m_B (M_{Sun})	q	a_{est} (AU)	SC ^b
I07364+0704	GJ 3454	AB	0.52 \pm 0.02	0.62 \pm 0.02	1000	10000	NY	0.18 \pm 0.03	0.14 \pm 0.01	0.81 \pm 0.07	5.8	Y
I08286+6602	—	AB	0.74 \pm 0.03	0.91 \pm 0.09	300	1000	MY	0.15 \pm 0.02	0.11 \pm 0.01	0.74 \pm 0.02	4.9	Y
I08316+1923	CU Cnc	AaAb	4.26 \pm 0.78	4.67 \pm 0.94	30	300	VY	0.20 \pm 0.09	0.04 \pm 0.03	0.20 \pm 0.09	6.0	Y
I08316+1923	CU Cnc	BaBb	0.55 \pm 0.00	0.63 \pm 0.01	30	300	VY	0.24 \pm 0.12	0.18 \pm 0.09	0.73 \pm 0.02	10.6	Y
I08563+1239	G 41-8	AB	0.40 \pm 0.01	0.51 \pm 0.01	30	300	VY	0.13 \pm 0.08	0.11 \pm 0.06	0.82 \pm 0.05	27.0	N
I08582+1945N	LHS 2077	AB	0.41 \pm 0.01	0.50 \pm 0.01	1000	10000	NY	0.13 \pm 0.03	0.11 \pm 0.02	0.88 \pm 0.02	9.6	Y
I09156-1035	LHS 6167	AB	1.18 \pm 0.07	1.43 \pm 0.06	30	300	VY	0.15 \pm 0.04	0.09 \pm 0.03	0.57 \pm 0.05	1.0	Y
I09218+4330	GJ 3554	AB	0.80 \pm 0.03	0.83 \pm 0.05	300	1000	MY	0.30 \pm 0.06	0.21 \pm 0.04	0.71 \pm 0.01	14.8	Y
I09256+6329	G 235-25	AB	1.52 \pm 0.11	1.41 \pm 0.07	1000	10000	NY	0.21 \pm 0.04	0.13 \pm 0.02	0.59 \pm 0.05	2.4	N
I09461-0425	LHS 2186	AB	0.36 \pm 0.01	0.39 \pm 0.01	1000	10000	NY	0.24 \pm 0.07	0.20 \pm 0.06	0.85 \pm 0.01	18.9	N
I12130+2146	—	AB	1.74 \pm 0.09	2.03 \pm 0.10	1000	10000	NY	0.24 \pm 0.08	0.12 \pm 0.03	0.50 \pm 0.05	4.7	Y
I14170+3142	GJ 3839	AB	0.55 \pm 0.03	0.61 \pm 0.06	300	1000	MY	0.43 \pm 0.03	0.33 \pm 0.03	0.76 \pm 0.02	7.1	Y
I15126+4543	GJ 3898	AB	1.57 \pm 0.10	1.75 \pm 0.10	300	1000	MY	0.30 \pm 0.06	0.15 \pm 0.03	0.51 \pm 0.01	9.9	Y
I15297+4252	LHS 3075	AB	1.29 \pm 0.05	1.56 \pm 0.06	1000	10000	NY	0.24 \pm 0.07	0.14 \pm 0.04	0.61 \pm 0.03	11.2	Y
I16280+1533	G 138-33	AB	1.75 \pm 0.08	1.70 \pm 0.07	1000	10000	NY	0.45 \pm 0.13	0.23 \pm 0.06	0.50 \pm 0.01	13.6	Y
I17076+0722	GJ 1210	AB	1.15 \pm 0.06	1.14 \pm 0.06	1000	10000	NY	0.21 \pm 0.06	0.13 \pm 0.03	0.62 \pm 0.03	5.6	Y
I18411+2447S	GJ 1230	AB	2.06 \pm 0.00	2.24 \pm 0.00	30	300	VY	0.40 \pm 0.18	0.12 \pm 0.03	0.33 \pm 0.08	40.0	Y
I19500+3235	LHS 3489	AB	1.42 \pm 0.19	1.38 \pm 0.18	1000	10000	NY	0.34 \pm 0.03	0.19 \pm 0.01	0.56 \pm 0.04	3.8	Y
I20021+1300	—	AB	1.35 \pm 0.02	1.38 \pm 0.03	1000	10000	NY	0.41 \pm 0.11	0.22 \pm 0.06	0.53 \pm 0.03	4.3	N
I20298+0941	HU Del	AB	2.72 \pm 0.23	—	30	300	VY	0.19 \pm 0.08	0.05 \pm 0.03	0.27 \pm 0.05	1.4	Y
I20300+0023	—	AB	1.34 \pm 0.05	1.59 \pm 0.06	1000	10000	NY	0.28 \pm 0.07	0.16 \pm 0.03	0.57 \pm 0.05	6.7	N
I20314+3833	LHS 3559	AB	1.69 \pm 0.57	1.49 \pm 0.37	1000	10000	NY	0.21 \pm 0.04	0.13 \pm 0.02	0.59 \pm 0.05	1.8	Y
I20337+2322	G 186-29	AB	1.33 \pm 0.00	—	1000	10000	NY	0.46 \pm 0.13	0.28 \pm 0.09	0.59 \pm 0.02	20.1	Y
I20488+1943	G 144-39	AB	1.70 \pm 0.03	1.75 \pm 0.07	1000	10000	NY	0.50 \pm 0.07	0.24 \pm 0.05	0.47 \pm 0.03	7.4	Y
I20593+5303	—	AB	1.53 \pm 0.41	1.76 \pm 0.45	1000	10000	NY	0.54 \pm 0.05	0.28 \pm 0.03	0.51 \pm 0.01	22.8	N
I21000+4004E	GJ 815	AB	1.79 \pm 0.08	1.86 \pm 0.08	30	300	VY	0.58 \pm 0.05	0.26 \pm 0.09	0.45 \pm 0.12	10.5	Y
I21013+3314	G 187-14	AB	0.76 \pm 0.04	1.07 \pm 0.06	1000	10000	NY	0.24 \pm 0.08	0.18 \pm 0.06	0.75 \pm 0.04	2.4	Y
I21014+2043	LHS 3610	AB	1.68 \pm 0.11	2.12 \pm 0.14	1000	10000	NY	0.25 \pm 0.04	0.13 \pm 0.02	0.50 \pm 0.05	8.9	N
I21173+2053N	G 145-31	AB	0.79 \pm 0.01	0.91 \pm 0.01	1000	10000	NY	0.21 \pm 0.08	0.15 \pm 0.05	0.71 \pm 0.03	93.9	Y
I21376+0137	—	AB	1.28 \pm 0.07	1.52 \pm 0.10	10	20	Sc12	0.11 \pm 0.04	0.05 \pm 0.02	0.45 \pm 0.01	5.2	Y
I21554+5938	—	AB	0.85 \pm 0.05	0.65 \pm 0.03	10	20	Sc12	0.14 \pm 0.07	0.09 \pm 0.05	0.57 \pm 0.11	2.7	Y
I22035+0340	—	AB	1.52 \pm 0.08	1.62 \pm 0.11	1000	10000	NY	0.24 \pm 0.10	0.13 \pm 0.04	0.55 \pm 0.06	6.8	Y
I22300+4851	—	AB	1.19 \pm 0.01	1.20 \pm 0.01	30	300	VY	0.44 \pm 0.20	0.25 \pm 0.13	0.56 \pm 0.08	42.7	Y

^aBasis for the age estimation.Sc12: Member of AB Dor or β Pic moving group according to Schlieder et al. (2012b).

Sh12: Estimated age in Shkolnik et al. (2012).

M13: Member of a young moving group according to Malo et al. (2013).

VY: Assumed very young based on high X-ray flux (as listed in Lépine & Gaidos 2011).

MY: Assumed moderately young based on moderate X-ray flux.

NY: Assumed not young based on lack of detectable X-ray flux.

^bFlag for whether targets is 'statistically clean' (Y) or not (N), see Sect. 6.1.